THERMAL BEHAVIOR AND PERFORMANCE OF LITHIUM-ION BATTERIES AT LOW TEMPERATURES

LITYUM İYON PILLERIN DÜŞÜK SICAKLIKLARDAKI ISIL DAVRANIŞI VE PERFORMANSI

ALTAY TEKİN

PROF. DR Murat KÖKSAL

Tez Danışmanı

Submitted to
Graduate School of Science and Engineering of Hacettepe University
as a Partial Fulfillment to the Requirements for the Award of the Degree of
Master of Sciences
in Mechanical Engineering

2023

ÖZET

LITYUM İYON PILLERIN DÜŞÜK SICAKLIKLARDAKI ISIL DAVRANIŞI VE PERFORMANSI

Altay TEKİN

Yüksek Lisans, Makine Mühendisliği Bölümü

Tez Danışmanı: Prof. Dr. Murat KÖKSAL

Mayıs 2023, 103 sayfa

Bu tezde bir ticari lithum iyon pillerin düşük sıcaklıklarda performansı ve ısıl davranışı deneysel olarak incelenmiştir. Özdeş piller üç farklı sıcaklık ortamında 0.5C ve 1.0C şarj ve deşarja tabii tutulmuştur. Ayrıca, düşük sıcaklık koşullarını benzetimlemek için şarj-deşarj deneylerinin yanısıra kurum içi bir 1—B elektrokimyasal-3-B termal birleşik model kullanılmıştır.

Bir pil test sistemi ile yapılan deneyler, sıcaklık düştükçe lityum iyon pillerin kapasitesi düşmekte ve pilin içindeki ısı üretimi artmakta olduğunu gösterdi. Model, oda sıcaklığında batarya voltajı ve yüzey sıcaklığını tahmin edebildi. Ancak, çalışma sıcaklığı azaldıkça, model ve deney sonuçları arasındaki hata artmaya başladı. Düşük sıcaklıklarda, lityum-iyon bataryaların elektrokimyasal özellikleri önemli ölçüde değişir. Sıcaklığa bağlı parametrelerin değişimlerinin etkilerini yakalayabilmek için -20°C'deki 1C deşarj deneyi verisi ile model tahminlerini karşılaştırarak bir duyarlılık analizi yapıldı. Duyarlılık analizi, sıcaklığı

azaltmanın özellikle elektrolit taşıma özellikleri üzerinde kötü bir etkiye sahip olduğunu gösterdi. Elektrolit difüzyon katsayısının, elektrolit taşıma sayısının, SEI film direncinin ve pilin özgül ısı kapasitesinin değişimi, model tarafından tahmin edilen batarya voltajı ve sıcaklığı üzerindeki en büyük etkiye sahip olduğu, ancak elektrotların difüzyon katsayısı, elektrolitin iyonik iletim katsayısı ve reaksiyon hızı katsayılarının daha az etkisinin olduğu gösterilmiştir. Sonuçlar aynı zamanda model parametrelerinin sıcaklığa bağlı olarak karakterizasyonunun daha doğru tahmin almak için kritik olduğunu göstermektedir.

Anahtar Kelimeler: Lityum-iyon piller, elektrokimyasal-termal birleşik model, duyarlılık analizi, batarya özellikleri, düşük sıcaklıklar

ABSTRACT

THERMAL BEHAVIOR AND PERFORMANCE OF LITHIUM-ION BATTERIES AT LOW TEMPERATURES

Altay TEKİN

Master of Sciences, Department of Mechanical Engineering

Thesis Supervisor: Prof. Dr. Murat KÖKSAL

May 2023, 103 pages

In this thesis, the performance and thermal behavior of a commercial lithium-ion battery were investigated experimentally at low temperatures. Identical batteries are subjected to 0.5C and 1.0C charge-discharge at three different temperature settings (25 °C, 4 °C and -20 °C). Furthermore, an in-house 1-D electrochemical-3-D thermal coupled model was utilized to simulate the low temperature conditions along with the charge-discharge tests.

Experiments conducted with a battery test system show that as the temperature decreases, the available capacity of the lithium-ion batteries decreases, and heat generation inside the battery increases. The model is able to predict battery voltage and surface temperature at room temperature. However, as the operating temperature gets lower, the discrepancy between the model and the experimental data begins to increase. At low temperatures, the electrochemical properties of the lithium-ion batteries change drastically. To capture the effects of varying temperature dependent parameters, a sensitivity analysis was performed comparing the 1C experimental discharge data at -20°C with the model predictions. The sensitivity analysis indicates that decreasing temperature has

negative effect especially on the electrolyte transport properties. It is demonstrated that while changing the electrolyte diffusion coefficient, electrolyte transport number, SEI film resistance, and the specific heat capacity of the battery have the largest impact on the battery voltage and temperature predicted by the model, electrode diffusion coefficient, electrolyte ionic conduction coefficient, and reaction rate constants have less impact. Results also show that the temperature dependent characterization of the model parameters is crucial for more accurate predictions.

Keywords: Lithium-ion batteries, electrochemical-thermal coupled model, sensitivity analysis, battery properties, low temperature

ACKNOWLEDGEMENTS

First and foremost, I would like to express my deepest gratitude to my supervisors Dr. Murat Köksal and Dr. Özgür Ekici. Their enthusiasm and assistance through every step of this thesis have made me devote myself to my thesis completely. I have been always inspired by their comments and advice.

I am grateful to my committee members, Dr. Bora Maviş, Dr. Bilsay Sümer, and Dr. Onur Baş for their invaluable comments.

I would also like to offer my sincere thanks to Dr. Tanılay Özdemir for his endless support and friendship.

Finally, I am deeply grateful to my family and my friends for their love and encouragement.

TABLE OF CONTENTS

LIST OF FIGURES

LIST OF TABLES

NOMENCLATURE

Symbols

$a_{s,i}$	Electrode surface area
$a_{s,ne}$	Negative electrode surface area
$a_{s,pe}$	Positive electrode surface area
brug	Bruggeman coefficient
$brug_{ne}$	Negative electrode Bruggeman coefficient
$brug_{pe}$	Positive electrode Bruggeman coefficient
$brug_{sep}$	Separator Bruggeman coefficient
c	Concentration
c_p	Specific heat capacity of the battery
c_s	Solid phase concentration
$c_{s,ne}$	Negative electrode solid phase concentration
$c_{s,pe}$	Positive electrode solid phase concentration
c_l	Liquid phase concentration
$c_{l,ne}$	Negative electrode liquid phase concentration
$c_{l,pe}$	Positive electrode liquid phase concentration
D_s	Solid phase diffusion coefficient
$D_{s,ne}$	Negative electrode solid phase diffusion coefficient
$D_{s,pe}$	Positive electrode solid phase diffusion coefficient
D_l	Liquid phase diffusion coefficient
D_l^{eff}	Effective liquid phase diffusion coefficient
$D_{l,ne}$	Negative electrode liquid phase diffusion coefficient

$D_{l,pe}$	Positive electrode liquid phase diffusion coefficient
E_a	Activation energy in Arrhenius equation
E_{eq}	Equilibrium potential
f_{+-}	Activity coefficient of ions
G	Gibbs energy
H	Enthalpy
h	Convective heat transfer coefficient
I	Applied current
I_{app}	Applied current density
J	Volumetric reaction rate
J_{ne}	Volumetric reaction rate at the anode
J_{pe}	Volumetric reaction rate at the cathode
J_0	Exchange current density
$J_{0,ne}$	Exchange current density at the anode
$J_{0,pe}$	Exchange current density at the cathode
k_a	Anodic reaction rate constant
k_c	Cathodic reaction rate constant
k_{th}	Thermal conduction coefficient of the battery
L_{ne}	Negative electrode thickness
L_{pe}	Positive electrode thickness
L_{sep}	Separator thickness
L_{tot}	Total thickness
n	Number of electrons
$\dot{Q}$	Heat generation
$\dot{Q}_j$	Joule heat generation
$\dot{Q}_{tot}$	Total heat generation

R_{SEI}	SEI film resistance
r	Radial direction in active material
r_{ne}	Radial direction in negative electrode active material
r_{pe}	Radial direction in positive electrode active material
S	Entropy per mol of lithium ions
T	Temperature
T_{amb}	Ambient temperature
T_s	Battery surface temperature
t	Time
t_+	Electrolyte transport number of ions
V	Voltage

Constants

F	Faraday constant
R	Ideal gas constant

Greek Symbols

α	Charge transfer coefficient
α_a	Anodic charge transfer coefficient
α_c	Cathodic charge transfer coefficient
ε	Emissivity
ε_l	Liquid phase volume fraction
$\varepsilon_{l,ne}$	Negative electrode liquid phase volume fraction
$\varepsilon_{l,pe}$	Positive electrode liquid phase volume fraction
$\varepsilon_{l,sep}$	Separator liquid phase volume fraction
ε_s	Solid phase volume fraction

$\varepsilon_{s,ne}$	Negative electrode solid phase volume fraction
$\varepsilon_{s,pe}$	Positive electrode solid phase volume fraction
$\varepsilon_{s,sep}$	Separator solid phase volume fraction
η	Overpotential
ρ	Battery density
σ_l	Ionic conduction coefficient
σ_l^{eff}	Effective ionic conduction coefficient
$\sigma_{l,ne}$	Ionic conduction coefficient at the negative electrode
$\sigma_{l,pe}$	Ionic conduction coefficient at the positive electrode
σ_s	Electrical conduction coefficient
σ_s^{eff}	Effective electrical conduction coefficient
$\sigma_{s,ne}$	Negative electrode electrical conduction coefficient
$\sigma_{s,pe}$	Positive electrode electrical conduction coefficient
Φ_l	Liquid phase potential
$\Phi_{l,ne}$	Liquid phase potential at the negative electrode
$\Phi_{l,pe}$	Liquid phase potential at the positive electrode
Φ_s	Solid phase potential
$\Phi_{s,ne}$	Solid phase potential at the negative electrode
$\Phi_{s,pe}$	Solid phase potential at the positive electrode
Ω	Ohm

Subscripts - Superscripts

app	applied
a	anode
c	cathode
eff	efficient

i	i^{th} material (i=ne, pe, sep)
l	liquid
ne	negative electrode
pe	positive electrode
sep	separator
s	solid

Abbrevations

CC-CV	Constant Current-Constant Voltage
EC:EMC	Ethyl Carbonate-Methyl Ethyl Carbonate
ECM	Equivalent Circuit Model
EIS	Electrochemical Impedance Spectroscopy
LCO	Lithium Cobalt Oxide
LFP	Lithium Iron Phosphate
LMO	Lithium Manganese Oxide
MCMB	MesoCarbon MicroBeads
NCA	Nickel Cobalt Oxide
NCM	Nickel Cobalt Manganese
PCM	Phase Change Material
PNGV	a Partnership for a New Generation of Vehicle
P2D	Pseudo-2-Dimensional
SEI	Solid Electrolyte Interphase
SP	Single Particle
SOC	State of Charge
SOH	State of Health

1. INTRODUCTION

1.1. Introduction

Lithium-ion batteries are one of the world's most common means of energy storage. They are preferred because of their high energy storage capability, low calendar aging, and ease of use. From small house appliances to space operations, Li-ion batteries can be comfortably put to use. Because of their long cycling life as opposed to their predecessors such as carbon-zinc batteries, maintenance advantages also become noticeable. Despite all these advantages operating temperatures are mostly limited to -20°C. At -20°C, commercial lithium-ion batteries lose a crucial proportion of their energy capacity, almost 90%, depending on their chemical composition. At the same time, the thermal and electrical behaviors of the battery change entirely at low temperatures. Li-ion batteries' complex chemical structure has always been challenging in terms of thermal behavior, such that the chemical reactions occurring during operation cause the battery to heat up. Even though much of the heat can escape from the surface, low temperature operations make Li-ion batteries build up heat much faster.

In a battery pack, this can cause some problems. Since a battery pack consists of series and/or parallel-connected batteries, one poor battery cell might lead to a bigger section of batteries not functioning properly, or even worse, thermal runaway. Therefore, it is crucial to determine the behavior of a single battery cell in terms of both performance and thermal and later move on to designing a battery pack.

1.2. Working Principle and Structure of Li-ion Batteries

Lithium-ion batteries consist of several components. These are electrodes, electrolyte, separator, and current collectors. The electrodes, namely the cathode and the anode, are the main lithium storage elements. Lithium ions are deposited inside the porous structure of the electrodes. In a charged state, lithium ions are nested in the anode. While discharging, lithium ions move through the electrolyte to reach the cathode. The electrolyte serves as a medium for the lithium ions to move freely between the cathode and the anode. The separator in the middle of the structure prohibits the electrodes from touching each other, hence, eliminating the short circuits. In the meantime, the anode-side current collector gathers electrons from the anode and sends them to the external circuit, where they eventually arrive at the cathode-side current collector. The same procedure occurs in reverse order while discharging.

Figure 1.1 depicts the charge and discharge processes in a simple Li-ion battery schematic. Solid electrolyte interphase (SEI) and cathode electrolyte interphase (CEI) in Figure 1.1 are products of electrolyte reduction. These layers act as a barrier, protecting electrolytes from decaying further and counteract their own formation process. They also function as a resistance, contributing thermal behavior and electrical performance of the battery somewhat inversely. Even though they originate from the same process of electrolyte reduction, SEI and CEI are distinct to their relative electrodes in terms of both thickness and composition [1].

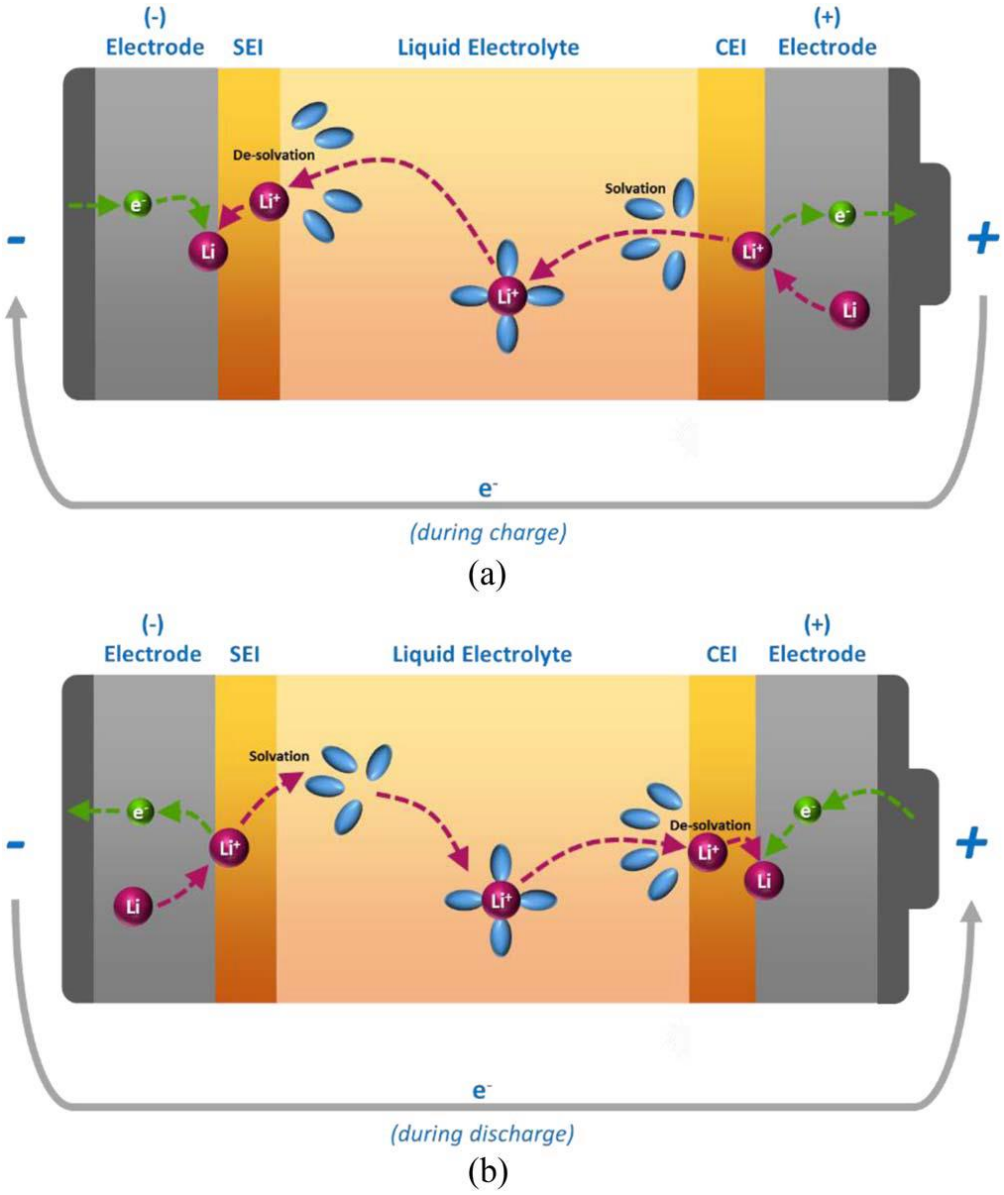

Figure 1.1. Li-ion Battery Structure, (a) Charge process. (b) Discharge process [1]

Two major electrochemical reactions are accountable for most of the battery's electrical performance. For the electrodes used in this study, NCA ($LiNiCoAlO_2$) cathode and graphite (LiC_6) anode, two electrochemical reactions are represented as below,

$$Li_xC_6 \underset{charge}{\overset{discharge}{\rightleftarrows}} C_6 + xLi + xe^- \quad \text{anode}$$

$$Li_{1-x}NiCoAlO_2 + xLi + xe^- \underset{charge}{\overset{discharge}{\rightleftarrows}} LiNiCoAlO_2 \quad \text{cathode}$$

$$Li_{1-x}NiCoAlO_2 + Li_xC_6 \underset{charge}{\overset{discharge}{\rightleftarrows}} LiNiCoAlO_2 + C_6 \quad \text{overall}$$

1.3. Thermal Behavior of Li-ion Batteries

Lithium-ion batteries can work under a wide range of conditions. Although, the capacity, power, and geometrical requirements of the user create some thermal challenges. Li-ion batteries heat up during both charge and discharge. Some of the heat is dissipated from the surface of the battery by convection and radiation. The remaining heat raises the battery temperature. Li-ion batteries are generally best utilized at temperatures between 20 and 40°C [2]. Temperatures above or below this range affect the battery performance, hence not preferred.

In 1985, Bernardi et. al. published one of the most widely used relations for heat generation [3]. This relation considers the heat generated from joule heating from electrical power, open circuit voltages (OCV), mixing of substances, and phase changes. Neglecting the heat of mixing and phase changes, it can be simplified into a simpler form as below,

$$\dot{Q} = I(OCV - V) - I\left(T\frac{\partial OCV}{\partial T}\right) \quad (1)$$

The first term on the right-hand side of the Eqn. (1) represents the Joule heating and is the reversible term in the heat generation equation, where (OCV-V) is overpotential. The second term on the right-hand side of the Eqn. (1) represents the heat generation due to entropy change and is the irreversible term. Like OCV

values, the entropic coefficient ($\frac{\partial OCV}{\partial T}$) is also dependent on the state of charge (SOC). In most studies, Eqn. (1) is employed in lithium-ion battery models [4-7].

At the same time, the heat generation equation can be rewritten using the Gibbs-Helmholtz equation as [8],

$$\dot{Q} = I^2R - IT\frac{\Delta S}{nF} \tag{2}$$

and Gibbs-Helmholtz equation is,

$$\Delta H = -T^2\frac{\partial}{\partial T}\left(\frac{\Delta G}{T}\right) = \Delta G + T\Delta S \tag{3}$$

where R denotes the equivalent or internal resistance of the battery, F is the Faraday constant, n is the number of electrons, and ΔS, ΔH, ΔG, represent entropy per mol of lithium ions, change of enthalpy, and Gibbs energy respectively. Some of the studies used this notation [9-11], since entropy can be measured with a calorimeter also.

However, in calorimetric measurements, the heat generation is measured as total rather than separate irreversible and reversible measurements. Studies showed that irreversible heat dominates the heat generated in the battery in high current operations or for batteries with high internal resistances [12, 13]. Nevertheless, reversible heat generation makes up a significant portion of the total heat generation for both charge and discharge and isn't always exothermic. Shi et al. [14] found that at the low C-rate of C/20 with the LMR cathode, reversible heat generation is almost always greater than irreversible heat generation, reaching five times the values observed during charging. Srinivasan et al. [15] overcharged batteries with the CC charging method and found out that anode reversible heat generation dominates the heat generation and is high enough to cause venting.

This current dependency of heat generation has caused researchers to sometimes neglect reversible heat generation in studies for simplicity [16]. On the other hand, some studies took the entropic coefficient as constant instead of taking it as a function of SOC [4].

1.4. Low Temperature Effect on Lithium-ion Batteries

In a series of experiments conducted by Nagasubramanian [17], 18650 Panasonic Li-ion cells lost 95% of their energy density when the temperature dropped from 35 to -40°C. Similarly, Zhang et al. [18] found out that the capacity of the assembled batteries underwent serious retention as the temperature decreased below -10°C. W. Wu et al. [19] investigated the effects of different discharge rates at -10°C cycling operations with the same charge rate and showed that lower discharge rates have a greater degradation effect on the battery capacity. Other studies with Li-ion batteries have shown similar effects when discharging at low temperatures.

But cycling or charging at low temperatures can lead to a more severe effect known as aging. H. Lin et al. [20] compared cycling Li-ion batteries at -10°C and -20C. Cells cycled at -10°C almost gained 100% of their relative capacity when returned to room temperature, but the capacity of the cells cycled at -20°C still had some loss when returned to room temperature. This behavior suggests that as the temperature gets lower, irreversible effects on capacity become more evident during cycling. Aging can be explained by anode voltage dropping below 0V relative to Li/Li^+ causing lithium ions to accumulate as metal at the anode surface known as lithium plating. High charging currents also aggravate lithium plating besides low temperatures [21]. The details of the aging and lithium plating will not be explained further as it is not a part of this study.

It was first believed that these problems when discharging are solely a result of temperature dependency of electrolyte properties. Therefore, research was conducted investigating subjects such as electrolytes with high ionic conductivity

and low freezing points [22-24]. Herreyre et al. [22] tried ethyl acetate and methyl butyrate as new solvents in graphite/$LiCoO_2$ cells. Both new solvents showed high performances at temperatures as low as -40°C. Smart et al. [23] focused on low ethylene carbonate (EC)-content electrolytes using different combinations of carbonate solvents EC, DEC, DMC, EMC, and different concentrations of $LiPF_6$ salt in the cells with MCMB-$Li_xNi_yCo_{1-y}O_2$ electrodes. They found out that electrolyte composition greatly influences discharge capacity at low temperatures. Li et al. [24] showed that changing the salt from $LiPF_6$ to $LiBF_4$ decreases polarization for graphite/Li half-cells but increases polarization for $LiFePO_4$/Li cells. However, since the polarization of graphite is bigger than $LiFePO_4$, $LiBF_4$ can still be favorable at low temperatures in $LiFePO_4$/graphite cells.

Electrolyte studies certainly improved the low temperature characteristics of Li-ion batteries but later studies showed that electrolyte conductivity has less effect on cell performance than initially assumed. The aforementioned study by Zhang et al. [18] showed that at low temperatures, charging a battery is more difficult than discharging according to electrochemical impedance spectroscopy (EIS) analysis and also suggested that electrolyte conductivity cannot be the only reason of capacity decrease happening rapidly below -10°C, and concluded with increased charge transfer resistance (R_{ct}) is the main factor for the poor battery performance at low-temperatures. Figure 1.2 shows the charging and discharging differences for graphite/graphite and cathode/cathode cells. Charge transfer resistance is one of the resistances used in equivalent circuit models and represents the resistance of the Li^+ desolvation step at the anode solid electrolyte interphase (SEI) and cathode electrolyte interphase (CEI) during charge/discharge processes together with lithium diffusion into solid electrodes. Liao et al. [25] performed low-temperature electrochemical impedance spectroscopy (EIS) analysis on $LiFePO_4$ cathode and showed that R_{ct} increases with decreasing temperature, easily representable by an Arrhenius type equation. In another study, using the same equivalent circuit model to represent a battery

cell, Zhang et al. [26] also showed R_{ct} to make up almost 100% of the total resistance in the battery as the temperature gets below -20°C.

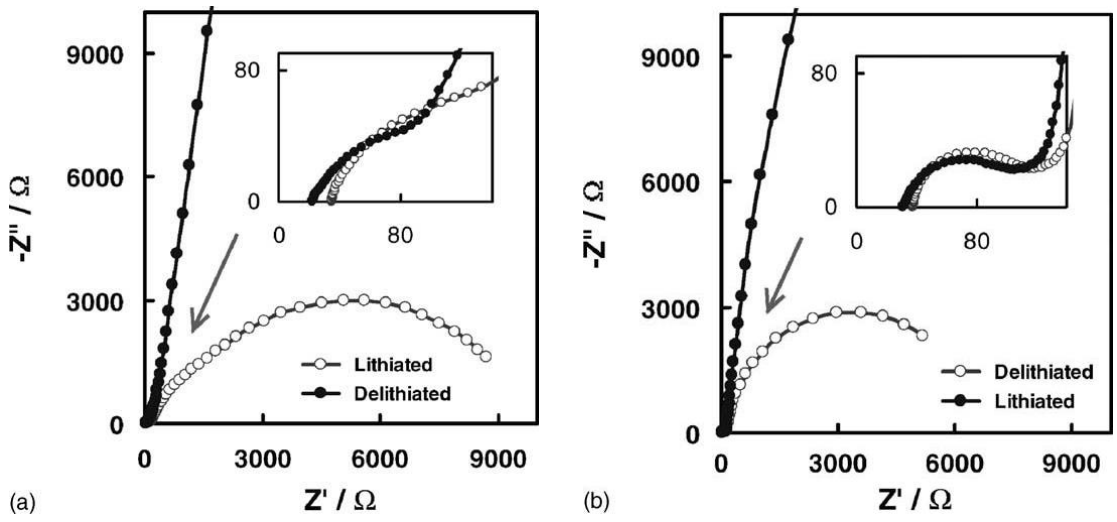

Figure 1.2. Lithiated and delithiated comparison with Nyquist plots of the symmetric cells (a) graphite/graphite and (b) cathode/cathode [14]

At the same time, other studies were carried out for battery thermal management systems as it is another possible solution to overcome low-temperature effects by heating the battery systems before operation. It can be achieved in three ways, through phase change materials (PCMs), external heating, and internal heating. PCMs are materials that have low melting points and higher energy storage capabilities. If the ambient temperature drops below PCM's melting point, the heat stored in PCM is transferred to the batteries. External heating systems use battery power to heat the fluids and then heated fluids to externally heat the battery packs. Generally, heater coils and fans are placed inside the battery pack. Fans blow heated air through batteries and heated air convectively warms the batteries. Vlahinos and Pesaran [27] compared the efficiency of some internal and external heating methods and showed computationally that internal core heating with resistive heating is more efficient than external heating methods. In internal heating, one way is the battery heating itself. Since at low temperatures, battery resistance is high, it is easier for a Li-ion battery to generate heat by directly drawing current. Wang et al. [28] designed a new battery structure by inserting a nickel foil into a prismatic battery, allowing the battery to warm up

quickly from -20°C to 0°C in 20 seconds (Figure 1.3). The second way is dividing the battery pack into two sections that are equal in capacity. One section is discharged to charge the other section, then vice versa. This procedure, named mutual pulse heating, allows most of the electrical energy to stay in the pack while gaining heat. The third case is to heat the battery by applying an external alternating current [29-31].

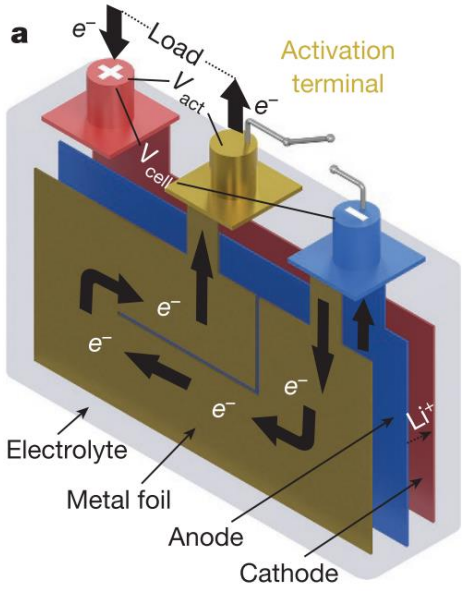

Figure 1.3. Self-heating battery with Nickel foil. A switch between the activation terminal and the negative terminal is controlling the self-heating mechanism. When the switch is “on” position, electrons move through Nickel foil, generating joule heat [28].

1.5. Aim and Scope of the Thesis

Commercial lithium-ion batteries have an optimal range of temperature to be operated. This range is determined by the manufacturer and generally is between -10°C and 45°C. However, as the areas of usage are expanding, lithium-ion batteries are needed to be operational at low temperatures. Although many successful research has been conducted for counteracting the low temperature effects by altering and improving the battery components, investigating the

temperature dependency of the electrochemical battery properties is still a growing area of research. Moreover, numerical examination of such electrochemical properties at low temperatures could be helpful for guiding new research in developing new battery components.

Thus, the aims of this thesis are,

1- Investigating the performance and thermal behavior of lithium-ion batteries under low temperature conditions.
2- Numerically investigating the sensitivity and the effects of changing temperature dependent parameters on the battery performance and thermal behavior.
3- Validating, and if needed improving, the available in-house mathematical model at low temperature conditions.

The scope of this study was limited to charging and discharging a cylindrical commercial lithium-ion battery at 25°C, 4°C, and -20°C and also doing sensitivity analysis on the discharge behavior of the lithium-ion battery with a few temperature dependent electrochemical parameters at -20°C.

2. MODELING

2.1. Models in Literature

Battery modeling methods can be represented under three main groups, equivalent circuit models, data-driven models, and electrochemical models. Battery models are used for estimating SOC, cell voltage, and remaining energy. Coupling with thermal models, one can also account for the temperature dependency of Li-ion battery performance while doing estimations.

2.1.1. Equivalent Circuit Models (ECM)

Equivalent circuit models represent the Li-ion batteries as electrical circuits. They have been used widely as it is simple to represent a Li-ion battery with circuit components, such as resistors and capacitors. ECMs are divided into two groups. Ones that are using time-domain and ones that are using frequency-domain. The most basic mode using the time domain, the Rint model, consists of a voltage source and a resistor. Adding combinations of resistors and capacitors, the Thevenin model, PNGV model, and GNL model can be constructed. In frequency-domain models, electrochemical impedance spectroscopy (EIS) is the most popular. Impedance spectra are obtained by applying a sinusoidal frequency of voltage. Through impedance spectra, researchers can gather information about chemical processes within the Li-ion battery. Overall, ECMs can represent the battery in a fast and robust manner with fewer model parameters, unlike other models.

2.1.2. Data-Driven Models

Data-driven models make use of big data sets to predict battery performance properties, such as state of health (SOH), state of charge (SOC), or voltage. They approach the battery as a black box, meaning the model doesn’t know what is happening inside the battery but knows it’s response to an input. In such models, mathematical algorithms, such as differential analysis methods, machine learning, and neural network, train a data set. Therefore, their capability of

estimating accurately any property is limited to the quality and the size of the data set.

2.1.3. Electrochemical Models

Physics-based electrochemical models usually consist of two big modeling approaches. One is the Single Particle (SP) Model and the other one is Pseudo-two-dimensional (P2D) Model developed by Doyle-Fuller-Newman. SP model is a simplified approach to an electrochemical system. It represents the electrodes as one big active material with no concentration gradients occurring inside the electrolyte and electrode, they behave uniformly. With the help of these assumptions, SP models can represent the batteries with less complex equations with fewer parameters. Therefore, it assures faster solving time but loses from accuracy.

The P2D model explains the electrochemical processes and battery components more extensively. Electrodes are represented as porous systems with multiple active particles. Both electrolyte and electrodes include the transport of the species with diffusion, mass transport, and charge transfer. The P2D model can represent the electrochemical system with a high degree of accuracy using concentration and potential distribution inside the battery components separately with partial differential equations. However, it comes with an extensive set of parameters to be determined by experiments and data fits. In other words, it requires more detailed knowledge about the electrochemical components individually. Such parameters that, are generally concentration and temperature dependent and also unique to the component's chemical composition. The complexity and variety of the parameters make the P2D model hard to utilize. As a result of the large number of partial differential equations and parameters, the P2D model has larger simulation times. Coupled with the thermal equations, the P2D model adapts the battery simulations to varying ambient temperatures. Coupled Electrochemical-Thermal model is explained in the next Chapter 2.2.

2.2. Electrochemical-Thermal Coupled Model

In this study, the 1-D electrochemical-3-D thermal coupled model developed by Özdemir using COMSOL was used [32]. Parameters in Özdemir's study are taken as a base model in this study. Özdemir's model has put together the geometrical, electrochemical, and thermal parameters of a cylindrical Li-ion battery with $LiNiCoAlO_2$ (NCA) cathode, graphite (MCMB) anode, EC:EMC (3:7) electrolyte with $LiPF_6$ salt, Al and Cu current collectors through some comprehensive inspection of literature. Some parameters, however, were not available for the same materials. In that case, parameters of relevant materials were used, as was often done in the literature.

2.2.1. Model Equations

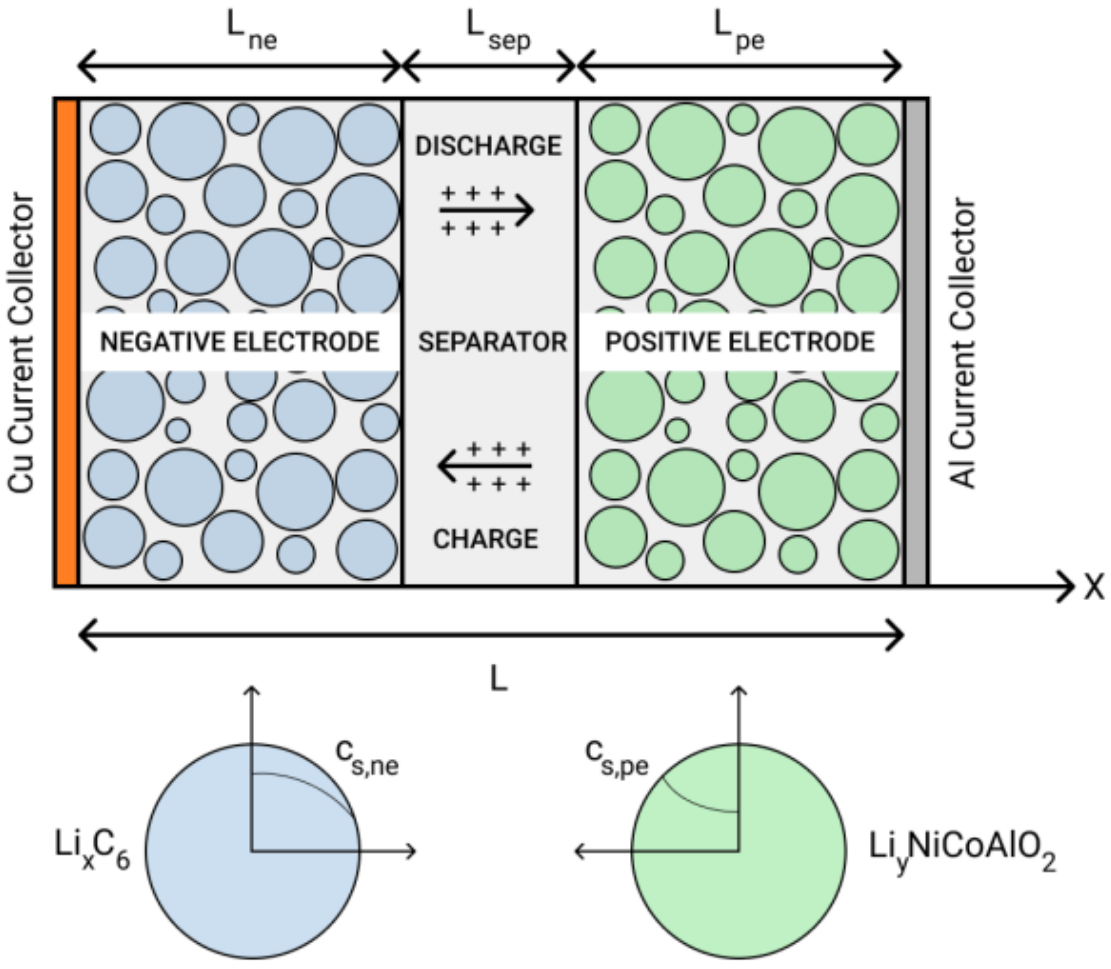

Figure 2.1. Lithium-ion battery P2D model structure [32]

Electrochemical models generally use Doyle-Fuller-Newman model equations also known as the pseudo-two-dimensional (P2D) model [33]. It is established from Newman and Tiedemann's porous electrode theory [34] and concentrated solution theory. Equations for the P2D model are as below,

First, mass balance in the solid phase is defined by,

$$\frac{\partial c_{s,i}}{\partial t} = \frac{1}{r_i^2}\frac{\partial}{\partial r_i}\left(r_i^2 D_{s,i}\frac{\partial c_{s,i}}{\partial r_i}\right) \tag{4}$$

where subscript i =positive electrode (pe), negative electrode (ne), and s=solid. D_s and c_s are solid phase diffusion coefficient and solid phase lithium-ion concentration respectively. In the denominators, r and t represent the radial direction in active material particles and time respectively. Boundary and initial conditions for mass balance,

$$-D_{s,i}\frac{\partial c_{s,i}}{\partial r_i}|_{r_i=R_{s,i}} = \frac{J_i}{a_s F} \qquad \frac{\partial c_{s,i}}{\partial r_i}|_{r_i=0} = 0 \tag{5), (6}$$

In Eqn. (5), $R_{s,i}$ represents the radius of the anode or cathode spherical particle, and J_i denotes the volumetric reaction rate at the surface of the active particle, a_s is electrode surface area and F is Faraday constant. Eqn. (5) describes the lithium flux at the surface of the active particle from liquid to solid. Eqn. (6) describes the no flux condition at the center of the active particle. Mass balance in the liquid phase is defined by,

$$\frac{\partial(\varepsilon_{l,i}c_l)}{\partial t} = \frac{\partial}{\partial x}\left(D_{l,i}^{eff}\frac{\partial c_l}{\partial x}\right) + \frac{J_i}{F}(1 - t_+) \tag{7}$$

where subscript l=liquid (electrolyte), t_+ denotes the transport number, sometimes also called as cationic transference number, of the electrolyte. In reality, however, the transference number is represented as T_+ and differs from the transport number. $\varepsilon_{l,i}$ is electrolyte volume fraction in the specific electrode. $D_{l,i}^{eff}$ represents the effective diffusion coefficient of the electrolyte, defined as below,

$$D_{l,i}^{eff} = (\varepsilon_{l,i})^{brug_i} \times D_{l,i} \tag{8}$$

where $brug_i$denotes the Bruggeman coefficient of the specific electrode with ***i*** = pe/ne. Boundary and initial conditions can be expressed as, Neumann boundary conditions, meaning no fluxes, at the ends of the domain (current collectors) in Eqn. (9) and Eqn. (10), and continuous fluxes between other interfaces in Eqn. (11) and Eqn. (12). At the same time, the separator does not block the movement of the lithium ions Eqn. (13) and Eqn. (14).

$$D_{l,ne}^{eff} \frac{\partial c_l}{\partial x}|_{x=0} = 0 \quad , \quad D_{l,pe}^{eff} \frac{\partial c_l}{\partial x}|_{x=L} = 0 \tag{9), (10}$$

$$D_{l,pe}^{eff} \frac{\partial c_l}{\partial x}|_{x=L_{ne}+L_{sep}} = D_{l,sep}^{eff} \frac{\partial c_l}{\partial x}|_{x=L_{ne}+L_{sep}} \tag{11}$$

$$D_{l,ne}^{eff} \frac{\partial c_l}{\partial x}|_{x=L_{ne}} = D_{l,sep}^{eff} \frac{\partial c_l}{\partial x}|_{x=L_{ne}} \tag{12}$$

$$c_l|_{x=L_{ne}^-} = c_l|_{x=L_{ne}^+} \tag{13}$$

$$c_l|_{x=(L_{ne}+L_{sep})^-} = c_l|_{x=(L_{ne}+L_{sep})^+} \tag{14}$$

The charge is conserved along the battery domain similar to mass. Charge balance in the solid phase can be expressed from Ohm's law,

$$\frac{\partial}{\partial x}\left(\sigma_{s,i}^{eff} \frac{\partial \phi_s}{\partial x}\right) = J_i \tag{15}$$

where ϕ_s denotes the potential of the solid phase at the particle surface, and $\sigma_{s,i}^{eff}$ is solid phase effective electrical conductivity. Similar to the effective diffusion coefficient, $\sigma_{s,i}^{eff}$ is defined as,

$$\sigma_{s,i}^{eff} = (\varepsilon_{s,i})^{brug_i} \times \sigma_{s,i} \tag{16}$$

where $\varepsilon_{s,i}$ and $\sigma_{s,i}$ are solid phase volume fraction and solid phase electrical conductivity of the related electrode, respectively. If an external current of I is applied, then the boundary condition at $x = L$ can be written as,

$$-\sigma_{s,pe}^{eff}\frac{\partial \phi_s}{\partial x}|_{x=L} = \frac{I}{A} = I_{app} \tag{17}$$

In Eqn. (17), A is the electrode area and I_{app} is applied current density. Charge cannot move through the separator as explained in Chapter 1. There are two boundary conditions to ensure this mathematically,

$$\sigma_{s,ne}^{eff}\frac{\partial \phi_s}{\partial x}|_{x=L_{ne}} = 0 \quad , \quad \sigma_{s,pe}^{eff}\frac{\partial \phi_s}{\partial x}|_{x=L_{ne}+L_{sep}} = 0 \tag{18), (19}$$

Eqn. (18) and Eqn. (19) state that charge flux is zero at both sides of the separator. Charge is also conserved in the liquid phase,

$$\frac{\partial}{\partial x}\left(-\sigma_l^{eff}\frac{\partial \phi_l}{\partial x} + \frac{2\sigma_l^{eff}RT}{F}\frac{\partial c_l}{\partial x}\left(1+\frac{\partial \ln f_{\pm}}{\partial \ln c_l}\right)(1-t_+)\right) = J_i \tag{20}$$

where ϕ_l denotes liquid phase potential, R is gas constant, T is the temperature in Kelvin. The expression $\left(1+\frac{\partial \ln f_{\pm}}{\partial \ln c_{l,i}}\right)$ is named thermodynamic factor (some studies named $\left(1+\frac{\partial \ln f_{\pm}}{\partial \ln c_l}\right)(1-t_+)$ as thermodynamic factor) where $f_{\pm}$ is molar activity coefficient of the electrolyte. σ_l^{eff} represents the effecitive conductivity of the electrolyte and similar to the Eqn. (8) and Eqn. (16), it can be expressed as,

$$\sigma_l^{eff} = (\varepsilon_l)^{brug_i} \times \sigma_l \tag{21}$$

where ε_l is liquid phase volume fraction and σ_l is electrolyte conductivity. Boundary conditions for the charge conservation in the liquid phase are,

$$\sigma_{l,ne}^{eff}\frac{\partial \phi_l}{\partial x}|_{x=0} = 0 \quad , \quad \sigma_{l,pe}^{eff}\frac{\partial \phi_l}{\partial x}|_{x=L} = 0 \tag{22), (23}$$

$$\phi_l|_{x=L_{ne}^-} = \phi_l|_{x=L_{ne}^+} \quad , \quad \phi_l|_{x=(L_{ne}+L_{sep})^-} = \phi_l|_{x=(L_{ne}+L_{sep})^+} \tag{24), (25}$$

$$\sigma_{l,ne}^{eff}\frac{\partial \phi_l}{\partial x}|_{x=L_{ne}^-} = \sigma_{l,sep}^{eff}\frac{\partial \phi_l}{\partial x}|_{x=L_{ne}^+} \tag{26}$$

$$\sigma_{l,sep}^{eff}\frac{\partial \phi_l}{\partial x}|_{x=(L_{ne}+L_{sep})^-} = \sigma_{l,pe}^{eff}\frac{\partial \phi_l}{\partial x}|_{x=(L_{ne}+L_{sep})^+} \tag{27}$$

The final consideration for the electrochemical model is intercalation kinetics, which is determined by the Butler-Volmer equation, Eqn. (28),

$$J_i = J_{0,i} a_{s,i} \left\{ exp\left(\frac{\alpha_a F}{RT}\eta\right) - exp\left(\frac{\alpha_c F}{RT}\eta\right) \right\} \tag{28}$$

$$J_{0,i} = F(k_a)^{\alpha_c}(k_c)^{\alpha_a}(c_{s,i})^{\alpha_c}(c_l)^{\alpha_a}(c_{s,i,max} - c_{s,i})^{\alpha_a} \tag{29}$$

$$\eta = \phi_s - \phi_l - E_{eq} \tag{30}$$

In Eqn. (28), α_a and α_c are the anodic and the cathodic charge transfer coefficients respectively. η is the overpotential and E_{eq} is the equilibrium potential, $a_{s,i}$ is the surface area of the respective electrode, and $J_{0,i}$ is the exchange current density. In Eqn. (29), k_a and k_c denote anodic and cathodic reaction rate constants respectively, and $c_{s,i,max}$ denotes the maximum lithium-ion concentration of the related electrode.

Together with the electrochemical equations, thermal equations provide knowledge about the thermal behavior of the cell. Further, parameters in electrochemical equations are generally highly temperature dependent. They are updated in every step with the cell temperature information coming from the thermal equation. Likewise, heat generation in the cell is determined by the Eqn. (1) with the voltage and current. Thus, the electrochemical part and thermal part create a coupling effect. We can start thermal equations by adding joule heating to the heat generation equation, Eqn. (31),

$$\dot{Q}_J = \left(\sigma_{s,i}^{eff}\frac{\partial^2 \phi_s}{\partial x^2}\right) + \\ + \frac{\partial \phi_l}{\partial x}\left(\sigma_l^{eff}\frac{\partial \phi_l}{\partial x} + \frac{2\sigma_l^{eff} RT}{F}\frac{\partial \ln c_l}{\partial x}\left(1 + \frac{\partial \ln f_{\pm}}{\partial \ln c_l}\right)(1 - t_+)\right) \tag{31}$$

Total heat generation becomes,

$$\dot{Q}_{tot} = J\eta - J\left(T\frac{\partial E_{eq}}{\partial T}\right) + \dot{Q}_J \tag{32}$$

Eqn. (33) represents the diffusion of the heat generated from the surface of the cell,

$$\rho c_p\left(\frac{\partial T}{\partial t}\right) = \dot{Q}_{tot} + \nabla(k_{th}\nabla T) \tag{32}$$

where, ρ is battery density, c_p is the specific heat capacity of the battery and k_{th} is the thermal conductivity of the battery. Heat is conducted from the center to the surface of the battery and then dissipated from the surface with natural convection and radiation. Eqn. (33) represents the boundary condition for the dissipation mechanism as,

$$k_{th}\nabla T = -h(T_s - T_{amb}) - \varepsilon\sigma({T_s}^4 - {T_{amb}}^4) \tag{33}$$

where, T_s is battery surface temperature, T_{amb} is the ambient temperature. The first term on the right-hand side represents the convective heat transfer with h being the convective heat transfer coefficient. The convective heat transfer coefficient is taken as temperature dependent with the Churchill-Chu correlation. The second term on the right-hand side represents radiation where ε is the emissivity and σ is the Stefan-Boltzmann constant.

2.2.2. Model Parameters

Base model parameters are adopted from [32]. The parameters which are thought to be temperature dependent are listed below. In this study, temperature dependent parameters were changed in the range of 20%, sometimes 30% to observe the effects better, for the -20°C, 1.0C model output. Effects of parameter changes were compared with the Root Mean Square Error (RMSE) analysis. Later, a combination of better parameters was investigated.

Table 2.1. Similar Values in the Literature for Negative Electrode Solid Phase Diffusion Coefficient.

Base Model Parameter	**Similar Values**	E_a (kJ/mol)	T_{ref} (K)
$D_{s,ne}$	1.87e-8*exp(-3936/T) [35]		
1.4523e-13* exp(68025.7/8.314*(1/318.15-1/T)) m^2/s	3e-13 [36]	40	298.15
	3.9e-14 [10, 37]	35	298.15
	2.55e-14(1.5-SOC)$^{3.5}$ [38]	50	298.15
	1.9e-15 [39]	35	258.15
	3.9e-14 [40]		

[10, 35-40]: Graphite

Table 2.2. Similar Values in the Literature for Positive Electrode Solid Phase Diffusion Coefficient.

Base Model Parameter	**Similar Values**	E_a (kJ/mol)	T_{ref} (K)
$D_{s,pe}$	4e-11 [35]		
3.5e-15* (1+tanh(-20*(SOC-0.73))+0.02) m^2/s	5e-13 [36]	30	298.15
	7.51e-14 [37]	31.556	298.15
	2e-14 [38]	25	298.15
	1e-13 [10]	20	258.15
	8e-14 [40]		

[35, 36, 38]: NMC, [10, 37]: LMO, [40]: LFP

Table 2.3. Similar Values in the Literature for Liquid Phase Ionic Conduction Coefficient.

Base Model Parameter	Similar Values
σ_l sigmal_int1(c)* exp(4000/8.314*(1/298.15-1/T)) S/m	$1198(c_l 10^{-3})^{-0.1882} \times (\exp[-0.9615 \log(c_l 10^{-3})^2] \times \exp(-2098/T)$ [35]
	$1.58 c_l \exp(0.85 c_l^{1.4})$ [38]
	$\sigma_{ref} \times \left(\frac{1.262(c_l/c_{ref})}{1+0.2(c_l/c_{ref})^2+0.08(c_l/c_{ref})^4} + 0.014\right)$ [40]
	$10^{-4} c_l(-10.5 + 0.074T - 6.69 \times 10^{-5} T^2 + 6.68 \times 10^{-4} c_l - 1.78 \times 10^{-5} c_l T + 2.8 \times 10^{-8} c_l T^2 + 4.94 \times 10^{-7} {c_l}^2 - 8.86 \times 10^{-10} {c_l}^2 T)^2$ [37, 41-43]
	$34.5 {c_l}^3 \exp(-798/T) - 485 {c_l}^2 \exp(-1080/T) + 2440 c_l \exp(-1440/T)$ [44]
	$10^{-3}(0.521 \times (1 + (T - 0.0228)) \times 10^{-3} c_l \times ((1 - 1.06\sqrt{10^{-3} c_l} + 0.353 \times (1 - 0.00359 \times \exp(1000/T)) \times 10^{-3} c_l)/(1 + (10^{-3} c_l)^4 \times (0.00148 \times \exp(1000/T)))))$ [45]

sigmal_int1: [46]
[38]: c_l (mol/cm^3), [40]: c_l (mol/dm^3), c_{ref} = 1 mol/dm^3
[45]: c_l (mol/L), σ (mS/cm), [44]: c_l (mmol/cm^3), σ (mS/cm)

Table 2.4. Similar Values in the Literature for Liquid Phase Diffusion Coefficient.

Base Model Parameter	Similar Values
D_l DL_int1(c)* exp(16500/8.314*(1/298.15-1/T)) m^2/s	$10\text{^}(-4.43 - \frac{54}{T-(229-5c_l)} - 0.22c_l)$ [37, 47, 48]
	$1.5 \times 10^{-10} exp\left[\frac{10000}{8.314}\left(\frac{1}{298.15} - \frac{1}{T}\right)\right]$ [38]
	$0.00584 {c_l}^2 \exp(-2870/T) - 0.0339 c_l \exp(-2920/T) + 0.129 \exp(-3200/T)$ [44]
	$1010 \exp(1.01 c_l) \times \exp(-1560/T) \times \exp(-487(c_l/T)) \times 10^{-6}$ [45]

DL_int1: [46]
[44]: c_l (mmol/cm^3), D_l (cm^2/s), [45]: c_l (mol/L), D_l (cm^2/s)

Table 2.5. Similar Values in the Literature for Bruggeman Coefficients.

Base Model Parameter	**Similar Values**		
$brugg_i$	Negative Electrode	Positive Electrode	Separator
	1.5 [37, 42, 49, 50]	1.5 [37, 42, 48-50]	1.5 [42]
$brugg_{ne} = 1.5$ $brugg_{pe} = 2.89$ $brugg_{sep} = 3.0$	2.9 [47]	2.4 [41]	2.3 [48]
	3.1 [41]	2.5 [42]	2.8 [47]
	4.0 [51]	2.8 [47]	3.2 [41]
	4.1 [48]	4.0 [51]	4.0 [37, 51]

Table 2.6. Similar Values in the Literature for Transport Number of the Electrolyte.

Base Model Parameter	**Similar Values**
t_+ transpNm_int1(c)	0.22 [40]
	0.26 [52]
	0.363 [35, 37]
	0.39 [41]
	0.41 [36]
	0.435 [48]
	$-0.000267{c_l}^2\exp(883/T) + 0.00309c_l\exp(653/T) + 0.517\exp(-49.6/T)$ [44]
	$-12.8 - 6.12c_l + 0.0821T + 0.904{c_l}^2 + 0.0318c_lT - 0.000127T^2 + 0.0175{c_l}^3 - 0.00312{c_l}^2 - 0.0000396c_lT^2$ [45]

transpNm_int1: [46]

[44]: c_l (mmol/cm^3), [45]: c_l (mol/L)

Table 2.7. Similar Values in the Literature for Activity Dependence of the Electrolyte.

Base Model Parameter	Similar Values
$f_{\pm}$	$0.00295\exp(-1720/T)$ [35]
$\left(1+\frac{\partial \ln f_{\pm}}{\partial \ln c_l}\right)(1-t_+)$	$0.601-0.24{c_l}^{0.5}+0.982[1-0.0052(T-294){c_l}^{1.5}]$ [10, 37, 41, 47]
$\left(1+\frac{\partial \ln f_{\pm}}{\partial \ln c_l}\right)$	$1.0442-0.0132{c_l}^{0.5}+0.5645{c_l}^{1.5}+0.09067T^{0.5}{c_l}^{1.5}-0.0055T{c_l}^{1.5}-0.0001T^{1.5}{c_l}^{1.5}$ [48]
actdep_int1(c)* exp(-1000/8.314*(1/298.15-1/T))	$0.540{c_l}^{2}\exp(329/T)-0.00225c_l\exp(1360/T)+0.341\exp(261/T)$ [44]
	$25.7-45.1c_l-0.177T+1.94{c_l}^{2}+0.295c_lT+0.000308T^{2}+0.259{c_l}^{3}-0.00946{c_l}^{2}T-0.000454c_lT^{2}$ [45]

actdep_int1: [46]

[10, 35, 37, 41, 47, 48]: $\left(1+\frac{\partial \ln f_{\pm}}{\partial \ln c_l}\right)(1-t_+)$, [44]: $\left(1+\frac{\partial \ln f_{\pm}}{\partial \ln c_l}\right)$, c_l (mmol/cm^3)

[10, 37, 41, 47]: c_l (mol/l), [48]: c_l (mol/m^3), [45]: c_l (mol/l)

Table 2.8. Similar Values in the Literature for Reaction Rate Constants.

Base Model Parameter	Similar Values			
k_a	Negative	Ea (kJ/mol)	Positive	Ea (kJ/mol)
1.764e-11	$1178\exp(-9237/T)$ [35]		$3.6\exp(-9616/T)$ [35]	
k_c	2.43e-11 [36]	45	1.02e-11 [36]	35
1e-10	1.764e-11 [37]	20	3.626e-11 [37]	32.7
mol$^{-1.5}$m$^{-0.5}$s^{-1}	7.77e-9 [53]		5.7e-8 [53]	

	2e-6 [10]	20	2e-6 [10]	53
	1.764e-11 [48]		6.7e-11 [48]	

[35, 36]: NMC-Graphite, [10, 37]:LMO-Graphite, [53]:NCA-Graphite

[48]:LCO-Graphite

[35, 53]: k ($m^{2.5}mol^{-0.5}s^{-1}$), [36, 37]: k (m/s)

[10]: k ($m^{2.5}mol^{-1.5}A$), [48]: k ($mol^{-1.5}m^{-0.5}s^{-1}$)

Table 2.9. Similar Values in the Literature for Specific Heat Capacity of the Battery.

Base Model Parameter	**Similar Values**
C_p	830 [54]
	896 [55]
750	950 [56]
	1090 [35]
J/kg.K	1720 [57, 58]

[35, 53-57]: C_p J/kg.K

Table 2.10. Similar Values in the Literature for SEI Film Resistance.

Base Model Parameter	**Similar Values**
R_{SEI}	100 [59]
	1e-3 [60]
0	20 [61]
Ω.m	3e-3 [50]

[59]: R_{SEI}: Ω.cm^2, [50, 60]: R_{SEI}: Ω.m^2, [61]: R_{SEI}: mΩ, [50, 59]: Changing with cycle #

3. EXPERIMENTAL SET-UP AND PROCEDURE

3.1. Charge-Discharge Tests

One of the fundamental points for testing with Li-ion batteries is to know how to handle charging and discharging procedures. In the literature, one can find different ways of charging and discharging schemes for specific purposes. For example, there are numerous studies to develop an optimal charging scheme in low temperature conditions [62, 63], so that the Li-ion batteries won't experience capacity degradation.

There are some limits within which a Li-ion battery should remain during charging and discharging for all types of schemes. These are cut-off voltage, a voltage value at which a battery is considered to be completely discharged, maximum voltage, a voltage value that can be reached at the end of the charging procedure and also called cut-off voltage, and temperature. These values for Panasonic 18650B Li-ion battery are obtained from the product datasheet [64] and presented in Table 1.

Table 3.1. Panasonic NCR18650B Li-ion Battery Specifications [64]

Specification	**Value**
Diameter	18.5 mm
Length	65.3 mm
Minimum capacity at 25°C	3250 mAh
Nominal voltage	3.6 V
Charge temperature	0 to +45°C
Discharge temperature	-20 to +60°C
Storage temperature	-20 to +50°C
Volumetric energy density	676 Wh/l
Gravimetric energy density	243 Wh/kg

In this study, the discharge procedure was chosen to be constant current (CC) discharging. A charged battery was discharged until the cut-off voltage of 2.5V was reached. For charging, constant current-constant voltage (CC-CV) pattern was employed. CC-CV is one of the most frequently used charging schemes in the literature [17, 65, 66]. As the name states, it consists of two distinct stages. First, a constant current was applied until the battery voltage reached 4.2V. Then, the battery testing system kept the voltage at 4.2V and tapered down the current until it reached 0.065A (C/50). All constant current parts were done with 0.5C and 1.0C. Where “C” or in other words “C-rate” represents the current, relating to the battery's capacity. 1C is equal to a current value that if it is applied for discharging the battery, it takes 1 hour to discharge to reach the cut-off voltage. The battery used in this study, Panasonic NCR18650B, has a 3250 mAh capacity which makes 1C equal to the 3250 mA or 3.25 A.

There were three separate temperatures investigated. The first series of tests were at room temperature (24-25°C) and done in a natural convection oven (Nüve FN300). The second series were carried out inside a refrigerator (Arçelik 4020T), and the temperature was set between 3-4°C. The last one is the focal point of this study, low temperatures. Low-temperature testing was done at -20°C. For this purpose, the freezer compartment of the same refrigerator is used. In all tests, cycling procedures were conducted with MACCOR 4300 test system. Batteries were connected with a T-type thermocouple from the middle of the battery surface for the temperature readings. Thermocouple data was recorded with a NI-DAQ device in all tests. Fig. 3.1. shows the MACCOR 4300 and Nüve FN300.

Figure 3.1. MACCOR 4300 (left) and Nüve FN300 (right)

3.2. Room Temperature Set-up

After securing the necessary connections with thermocouples and MACCOR 4300, batteries were placed and left in the oven for six hours to achieve a uniform temperature distribution in the battery. Fig. 3.2. shows battery connections and devices used in tests. After each discharge or charge procedure, batteries were left to rest for at least six hours to assure electrochemical stability. The detailed test procedure is explained in Fig. 3.3..

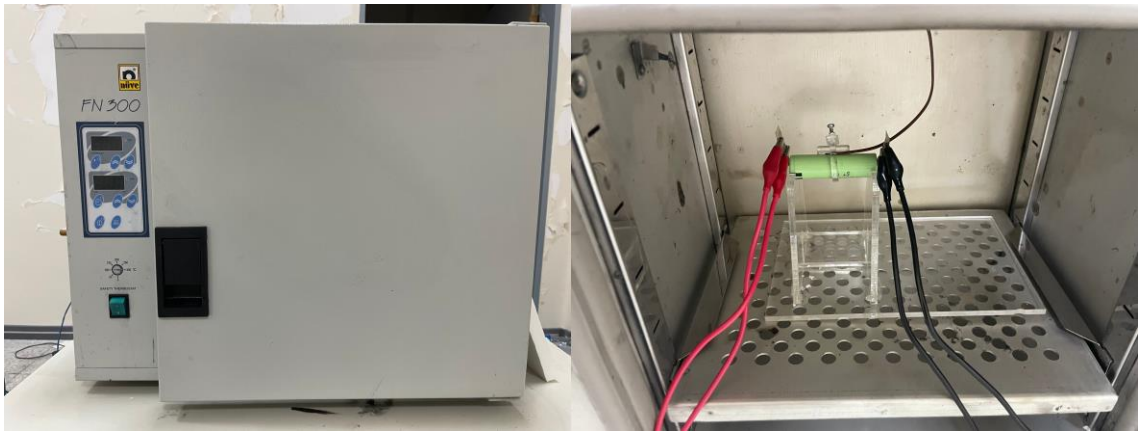

Figure 3.2. Battery connections and placement inside the oven.

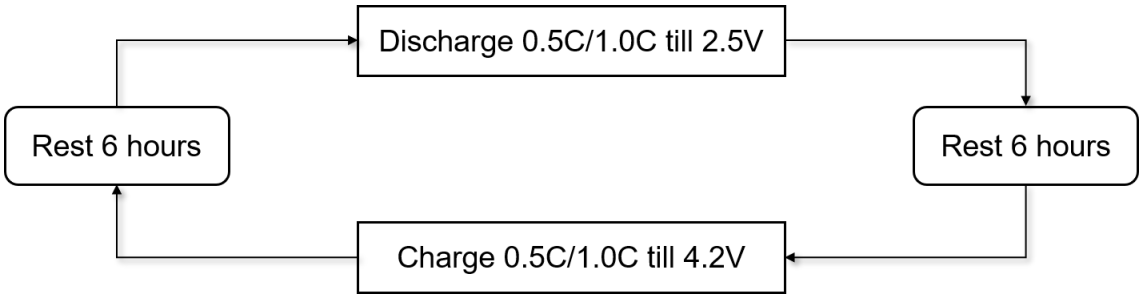

Figure 3.3. Room temperature test procedure.

3.3. Low Temperature Set-up

In low temperature tests, a commercial refrigerator was used. However, refrigerators are not capable of keeping the temperature constant for a long time. Significant temperature fluctuations were observed reaching up to ±5°C. For this reason, a few thermogel pads were placed inside a polystyrene foam box. Bottles filled with water were placed in the rest of the refrigerator. Higher heat capacity of the thermogels and water lowered the temperature fluctuations to be between ±1°C. Fig. 3.4. shows the refrigerator set-up for low temperature tests.

Low temperature operations have great tolls on Li-ion batteries as explained before in Chapter 1. As a half-way solution to these problems, battery operations can be divided. Instead of cycling repeatedly at low temperatures, batteries that were charged at low temperatures were discharged at room temperature and the batteries that were discharged at low temperatures, were charged at room temperature. While doing so, room temperature operations were carried out with 0.5C always. So, charging and discharging at low temperatures were investigated separately, with different batteries. Another problem with low temperature operation was high IR polarization caused by elevated charge transfer resistance. Because of the high IR polarization, the battery voltage reached the cut-off voltage immediately after low temperature operation has started. To overcome this problem, the cut-off voltage was overridden for 30 seconds after the start. Fig. 3.5. and Fig. 3.6. explains low temperature tests in detail.

Figure 3.4. Battery connections and placement inside the refrigerator.

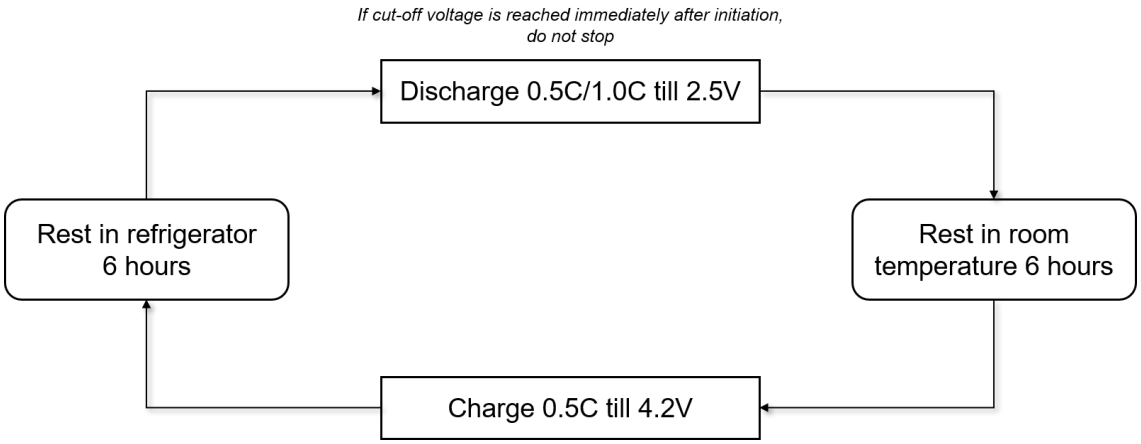

Figure 3.5. Discharge procedure at -20°C

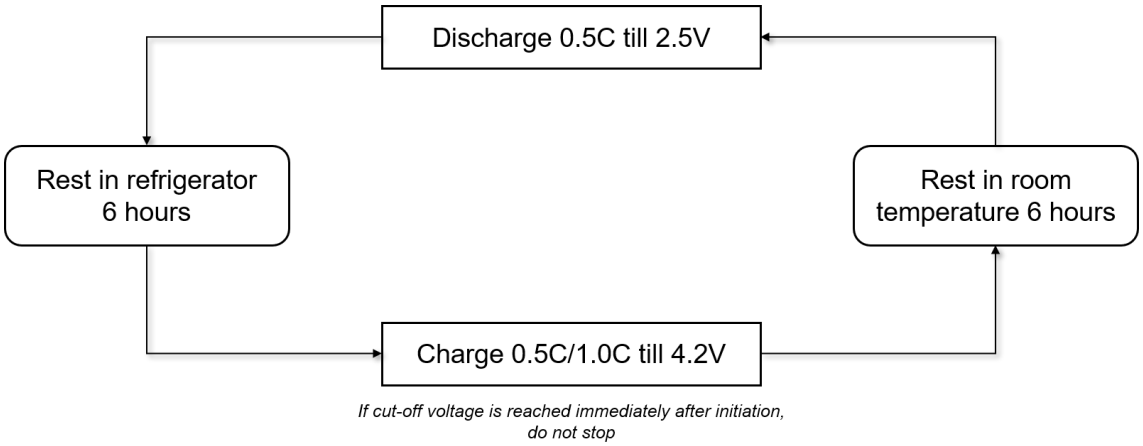

Figure 3.6. Charge procedure at -20°C

4. RESULTS AND DISCUSSION

4.1 Experimental Results

In order to assess the performance of a commercial NCR18650B battery, cells were charged and discharged at various temperatures. To compare the results, room temperature characteristics are taken as base performance values. Cells are charged and discharged according to the manufacturer's datasheet. Fig. 4.1. shows room temperature performance for 0.5C and 1.0C.

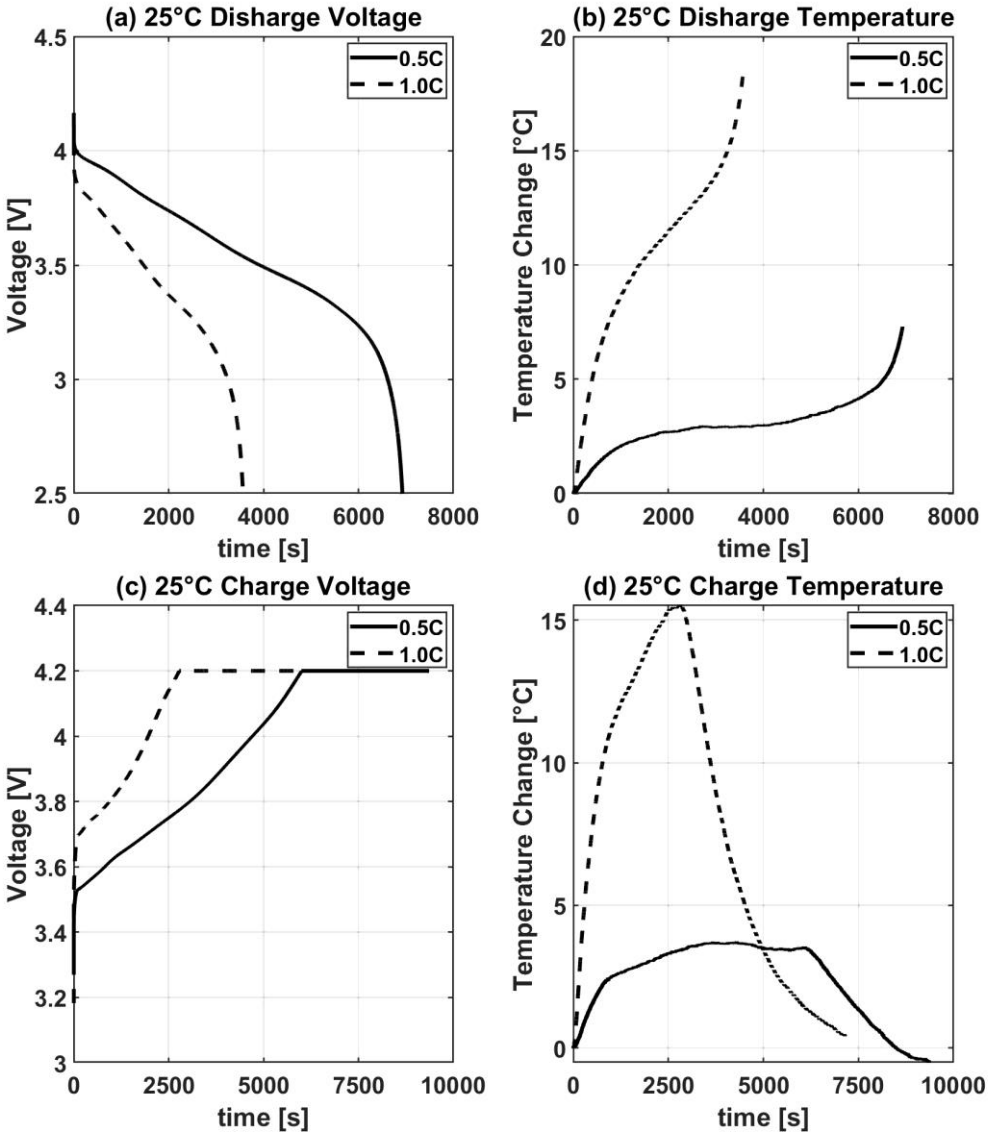

Figure 4.1. Discharge (a-b) and charge (c-d) tests results at 25°C.

Higher C-rates, per definition, cause the battery to deplete stored energy faster than lower C-rates while discharging, and charging the battery faster. In accordance with Eqn. (1), higher C-rates generate more heat, hence temperature rises quickly in the case of 1.0C for both charge and discharge, reaching up to 15°C difference in charge and 20°C difference in discharge. For the charging case, lower C-rates resulted in longer CV charging time.

As the temperature gets lower, available capacity in the battery is decreased, because of the sluggish electrochemical kinetics in the battery. In order to see the difference stepwise, some batteries were cycled at 3-4°C. Voltage and temperature differences in 3-4°C charge and discharge tests are presented in Fig. 4.2. below.

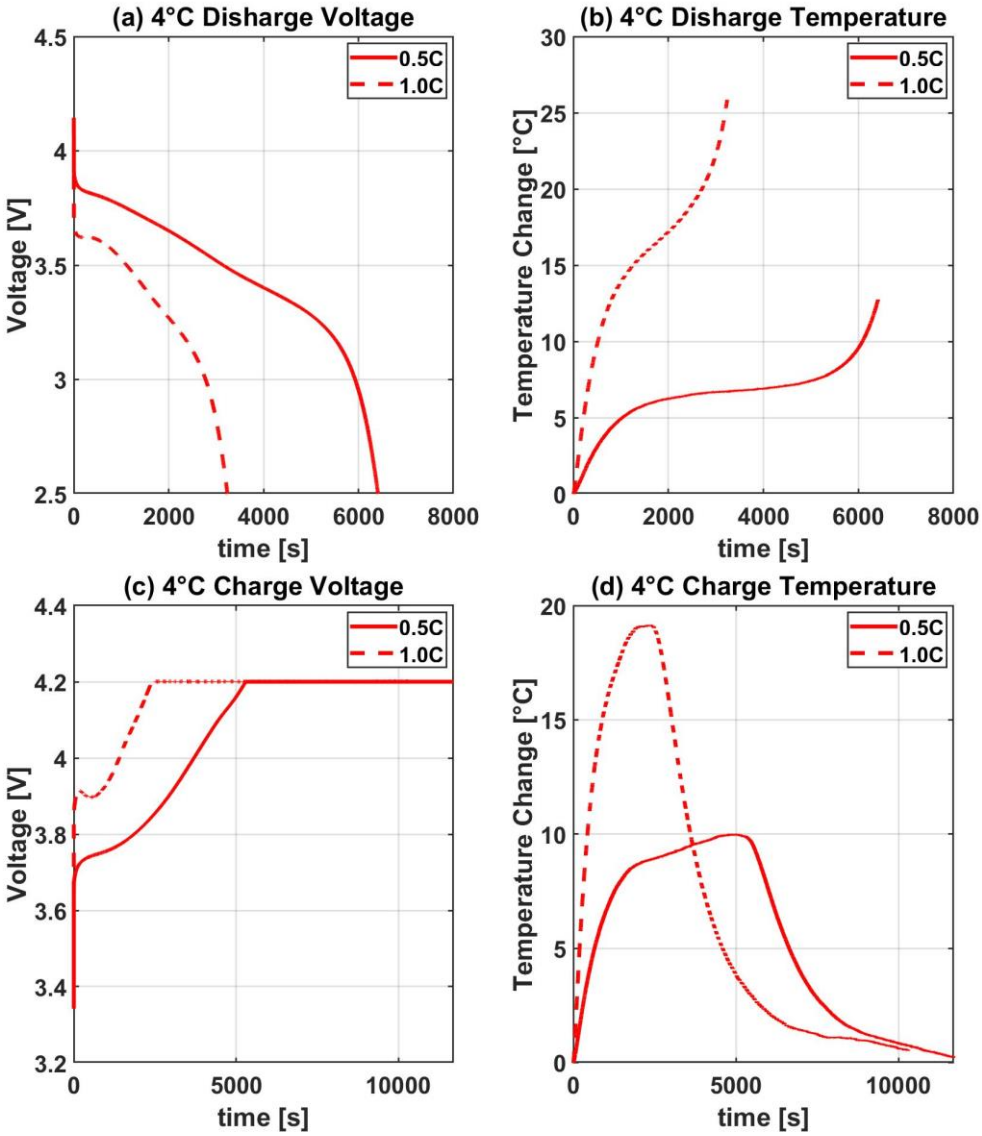

Figure 4.2. Discharge (a-b) and charge (c-d) tests results at 4°C.

Discharge and charge values in Fig. 4.2. a-c show greater voltage differences at the very initiation of the tests. Relatively higher charge transfer resistance causes IR (ohmic) polarization in the battery, which produces large overpotential. As a result of this large overpotential, the temperature gradient is higher, and eventually, the maximum temperature is higher in both charging and discharging. Operations at temperatures below 0°C have even greater visible changes in battery performance. -20°C tests are presented in Fig. 4.3..

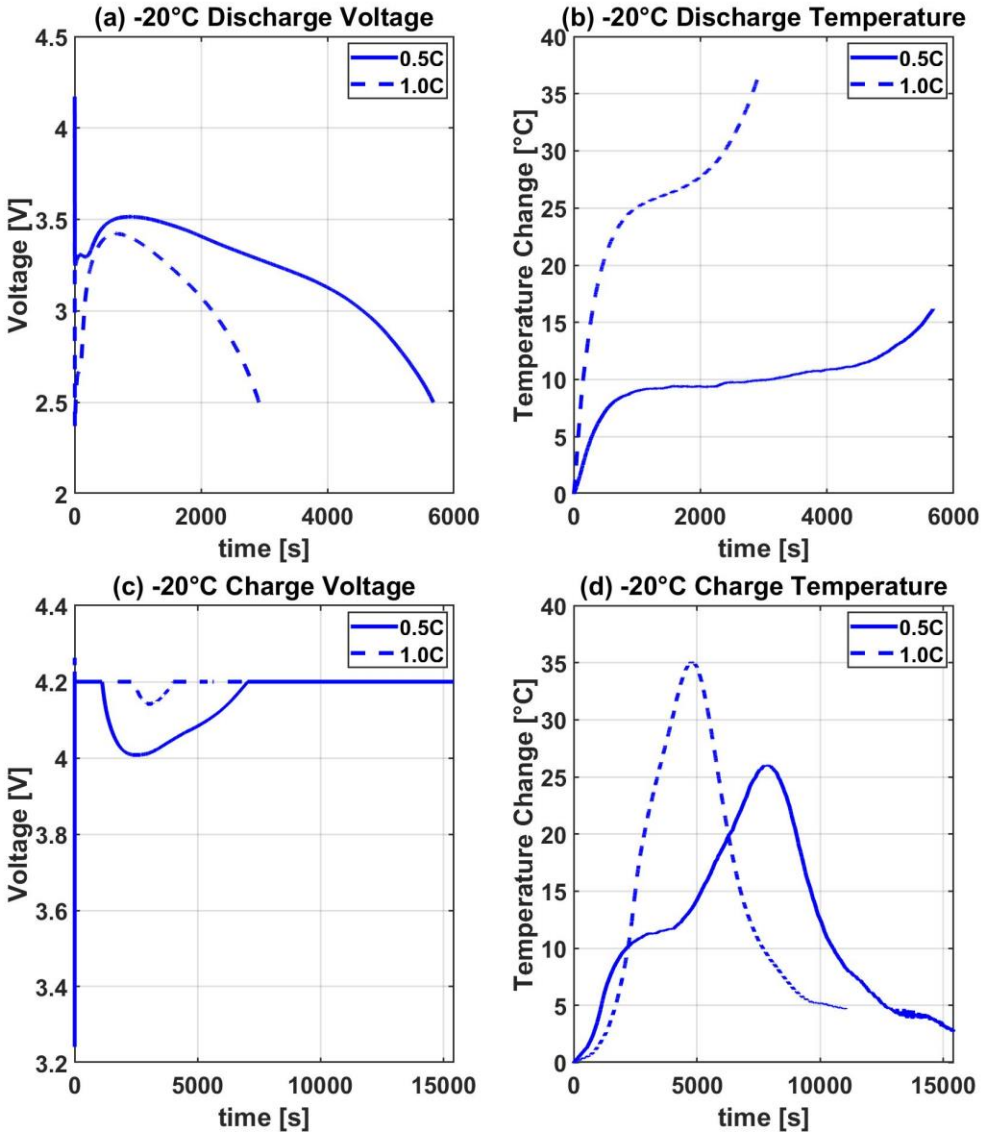

Figure 4.3. Discharge (a-b) and charge (c-d) tests results at -20°C.

In Fig. 4.3. (a) and (c), overpotentials are so high for the tests that the battery voltages immediately reach cut-off voltages, except for 0.5C discharge. In the charging process, this means that the CC part of charging is over and the CV part begins. In the CV part, the heat accumulates quickly because of the overpotentials. This heat, in return, drops the resistances caused by low temperatures and voltage begins to drop. For the 1.0C case, this period is shorter probably because of the lower diffusivity of negative electrode or lithium plating. In discharge, battery voltage displays a similar bounce. For the 1.0C test, the temperature rise in discharge is greater than that in charge, however for the 0.5C

test, long CC charge time along with higher voltages (>4V), generate more heat than 0.5C discharge.

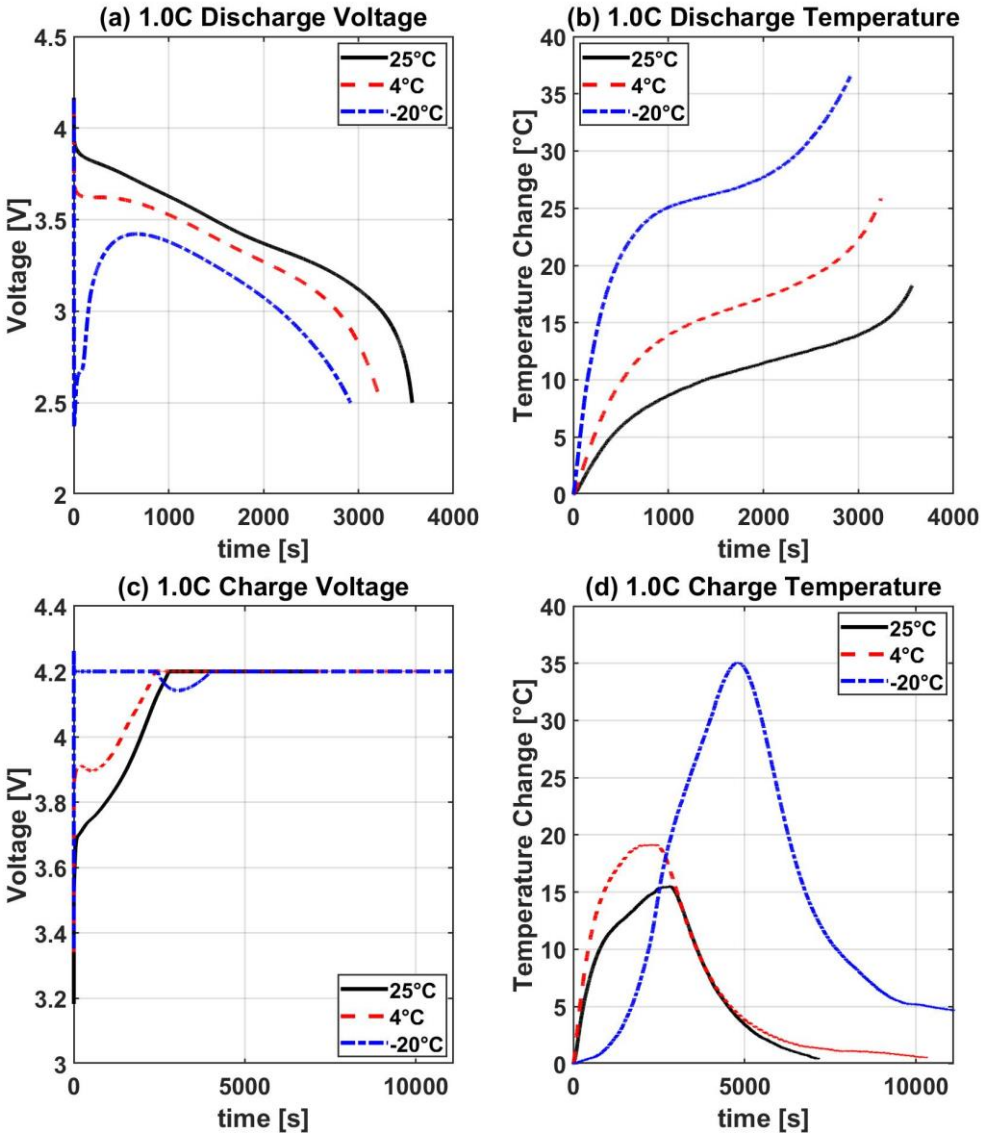

Figure 4.4. 1.0C discharge (a-b) and charge (c-d) tests results at 25, 4, and -20°C

Fig. 4.4. and Fig. 4.5. display the effects of different temperatures on the charge and discharge performances of the battery. As the temperature gets lower, discharge time gets shorter, discharge capacity gets lower, and temperature change increases as expected. It is clear that overpotential increases with decreasing temperature for both 0.5C and 1.0C operations.

Charging in both C-rates displays a peak in temperature. For the -20°C charge operations, the temperature rises even when the charging type is CV before the peak temperature. That is because the current rises before the peak temperature, leading to a higher heat generation as time goes by. After the peaks, charge operations in all temperature settings result in decreasing current over time.

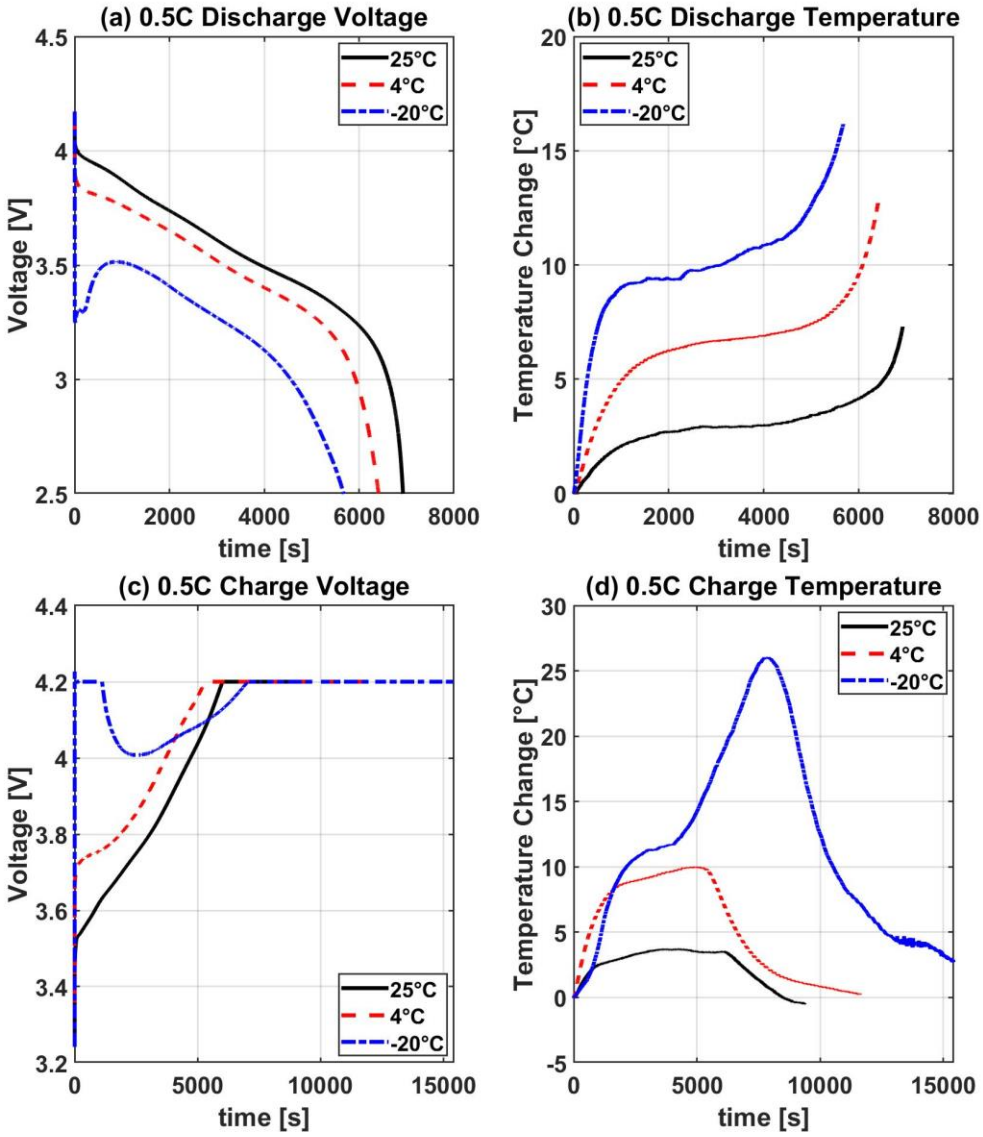

Figure 4.5. 0.5C discharge (a-b) and charge (c-d) tests results at 25, 4, and -20°C

4.2. Model Sensitivity Analysis

This part presents the results of varying different model parameters on the battery voltage and temperature. Base model parameters are changed with increments of 10%, 100% being the initial value in the model. Sensitivity analysis was carried out comparing the -20°C, 1C discharge experiment data with the model results for both the voltage and the temperature.

Table 4.1. Model Sensitivity Analysis on Battery Voltage.

	Percentage of Base Model Parameter and It's Effect on Voltage					
Parameter	%80	%90	%100	%110	%120	%130
$D_{s,ne}$	0.3960	0.3978	0.4004	0.4010	0.4021	-
$D_{s,pe}$	0.3947	0.3957	0.4004	0.4015	0.4031	-
D_l	0.7293	0.4476	0.4004	0.3304	0.3040	0.3223
σ_l	0.3769	0.3940	0.4004	0.4081	0.4153	-
$brugg_{ne}$	0.3505	0.3521	0.3540	0.3562	0.3573	-
$brugg_{pe}$	0.3169	0.3441	0.4004	0.4647	0.5229	-
$brugg_{sep}$	0.3623	0.3775	0.4004	0.4313	0.4506	-
t_+	0.4468	0.4228	0.4004	0.3775	0.3564	0.3376
$\frac{\partial \ln f_{\pm}}{\partial \ln c_l}$	0.4154	0.4074	0.4004	0.3924	0.3856	0.3794
C_p	0.3696	0.3831	0.4004	0.4192	0.4424	-
k_a	0.3933	0.3962	0.4004	0.4019	0.4041	-
k_c	0.3977	0.3986	0.4004	0.4004	0.4010	-
R_{SEI}	0.2586	0.2466	0.2355	0.2252	0.2155	

Table 4.2. Model Sensitivity Analysis on Battery Temperature

	Percentage of Base Model Parameter and It's Effect on Temperature					
Parameter	%80	%90	%100	%110	%120	%130
$D_{s,ne}$	8.8502	9.1144	9.3281	9.5290	9.6886	-
$D_{s,pe}$	9.1833	9.3044	9.3281	9.3981	9.4489	-
D_l	9.5686	7.8603	9.3281	9.1814	9.3970	9.9557
σ_l	8.5770	8.9381	9.3281	9.6084	9.8265	-
$brugg_{ne}$	10.5947	10.5179	10.4313	10.3356	10.1600	-
$brugg_{pe}$	9.7552	9.3562	9.3281	9.4383	9.5461	-
$brugg_{sep}$	9.6611	9.5372	9.3281	8.8941	7.9458	-
t_+	8.9266	9.1675	9.3281	9.4693	9.5816	9.6898
$\frac{\partial \ln f_{\pm}}{\partial \ln c_l}$	9.8961	9.6124	9.3281	9.0764	8.8235	8.5805
C_p	8.3237	8.8302	9.3281	9.8554	10.3683	-
k_a	9.1567	9.2644	9.3281	9.4148	9.4757	-
k_c	9.2565	9.3042	9.3281	9.3705	9.3972	-
R_{SEI}	5.9737	5.6188	5.2819	4.9612	4.6551	

4.2.1. Negative Diffusion Coefficient

The negative diffusion coefficient represents the lithium intercalation and deintercalation in the negative electrode. A higher diffusion coefficient accounts for better intercalation kinetics. Slower kinetics causes lithium to move slowly inside the electrode, resulting in a more uneven concentration gradient. The

diffusion coefficient in graphite anode is generally around 1e-13 m^2/s at room temperature (Table 2.1.) and it is a highly temperature dependent property. The figure below shows the simulation results for changes in the base diffusion coefficient in the model.

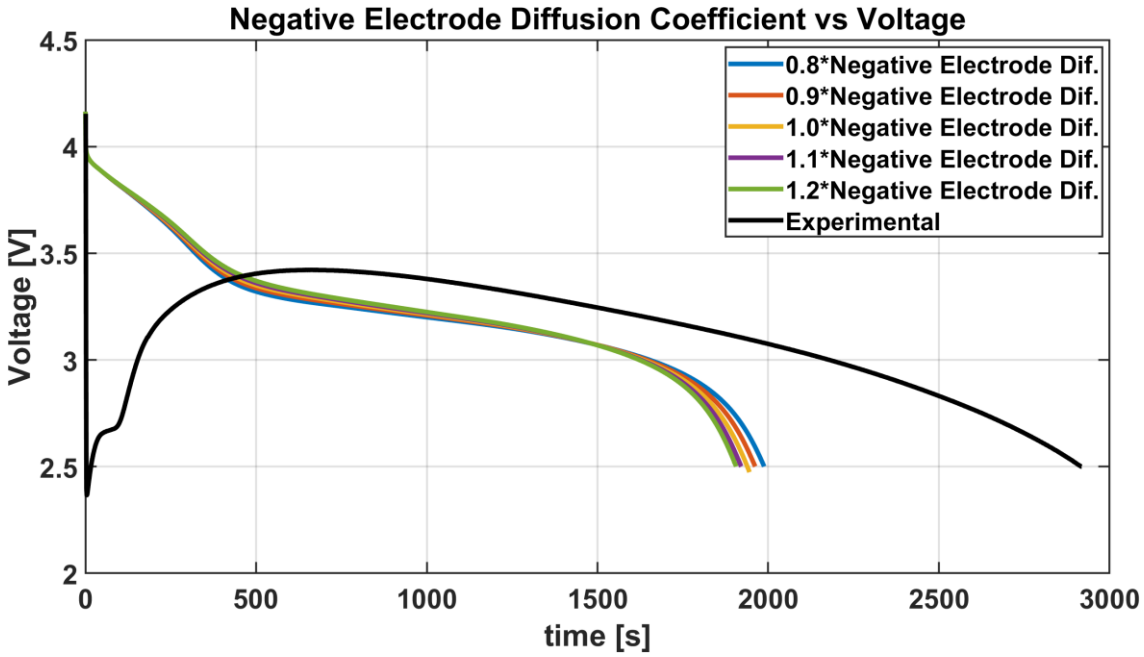

Figure 4.6. Negative Electrode Diffusion Coefficient vs Voltage

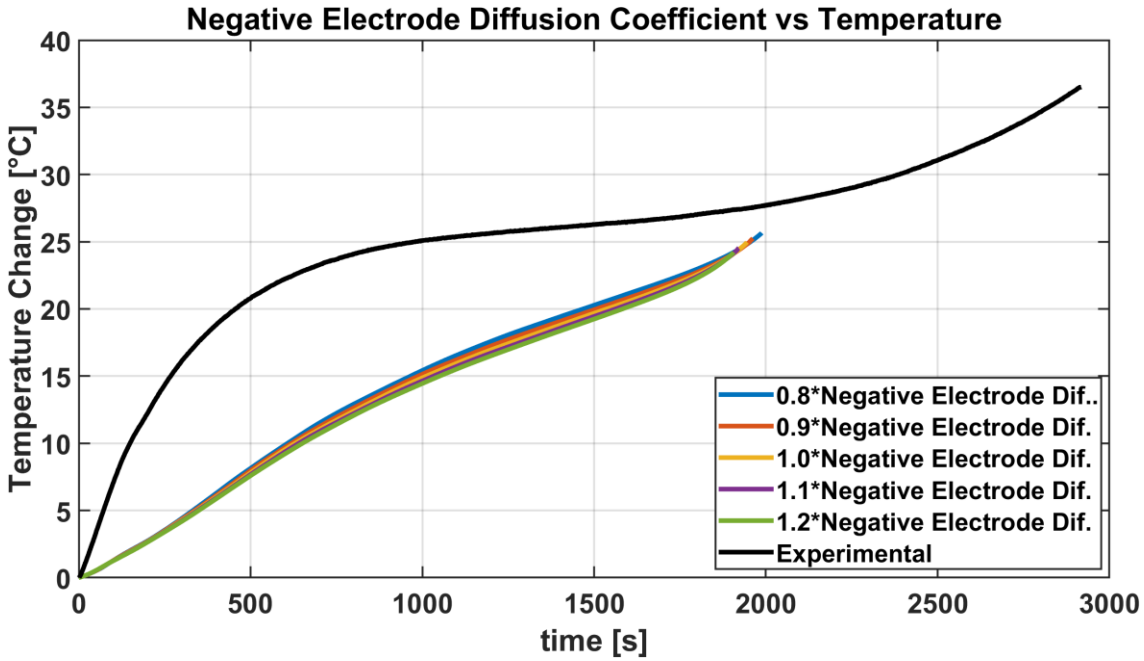

Figure 4.7. Negative Electrode Diffusion Coefficient vs Temperature

It is clear from Table 4.1. and Fig. 4.6. that lithium kinetics in anode could be taken a little slower in order to get closer to the experimental result, indicating a lower diffusivity. A lower diffusivity of 80% has improved both voltage and temperature estimation in simulations. Kulova et al. [39] investigated graphite diffusion in different temperatures and found that the diffusion coefficient of the graphite is 1.9e-15 m^2/s at -15°C, and decreases with decreasing temperature while our base model parameter is around 1.99e-16 m^2/s at -20°C. A decrease of 20% in the diffusion coefficient decreases the RMSE and helps the apparent simulation results but it's effects might be minimal at this state since the base model parameter can estimate similar graphite diffusivity at -20°C

For a blind estimation without numbers, we can say that low temperature decreases the lithium diffusivity in graphite anode.

4.2.2. Positive Diffusion Coefficient

Similar to graphite diffusivity, NCA diffusivity is adversely affected by decreasing temperature. However, positive electrodes are generally affected less than negative electrodes. A comparison between the diffusion coefficients in Table 2.1. and Table 2.2., can put forth the differences in the activation energies (E_a). The activation energy term in the Arrhenius equation represents the slope between log(D) and 1/T. Hence, a larger activation energy term means that decreasing temperature has a greater impact on the electrochemical property. Fig. 4.8. and Fig. 4.9. show the impact of modifying the positive electrode diffusivity on the battery voltage and temperature.

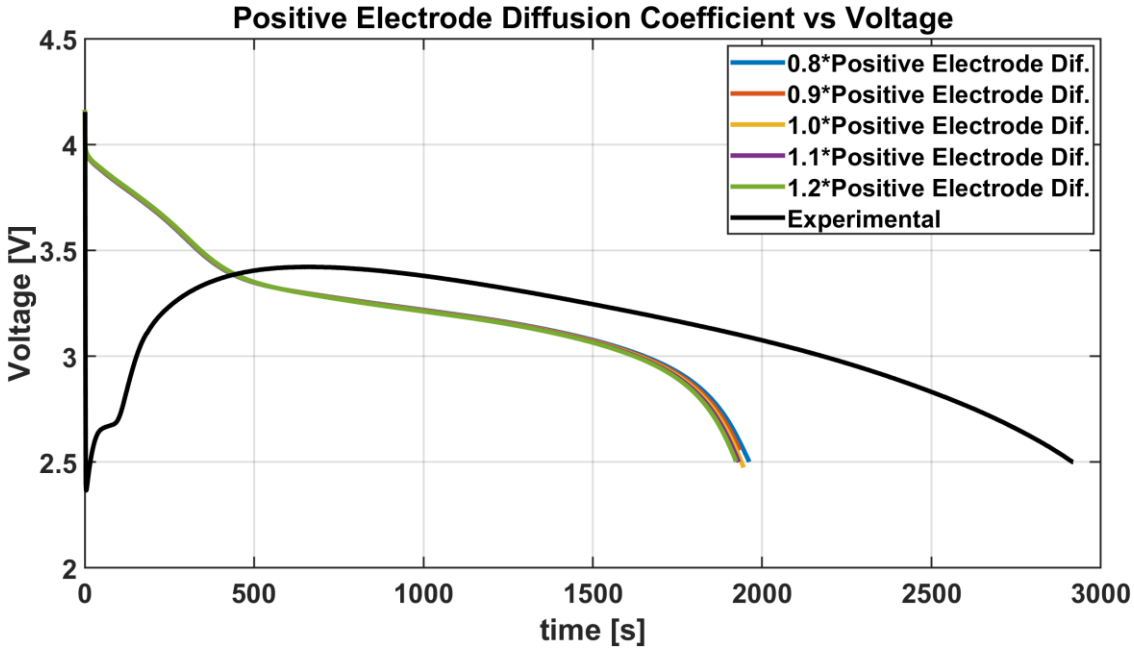

Figure 4.8. Positive Electrode Diffusion Coefficient vs Voltage

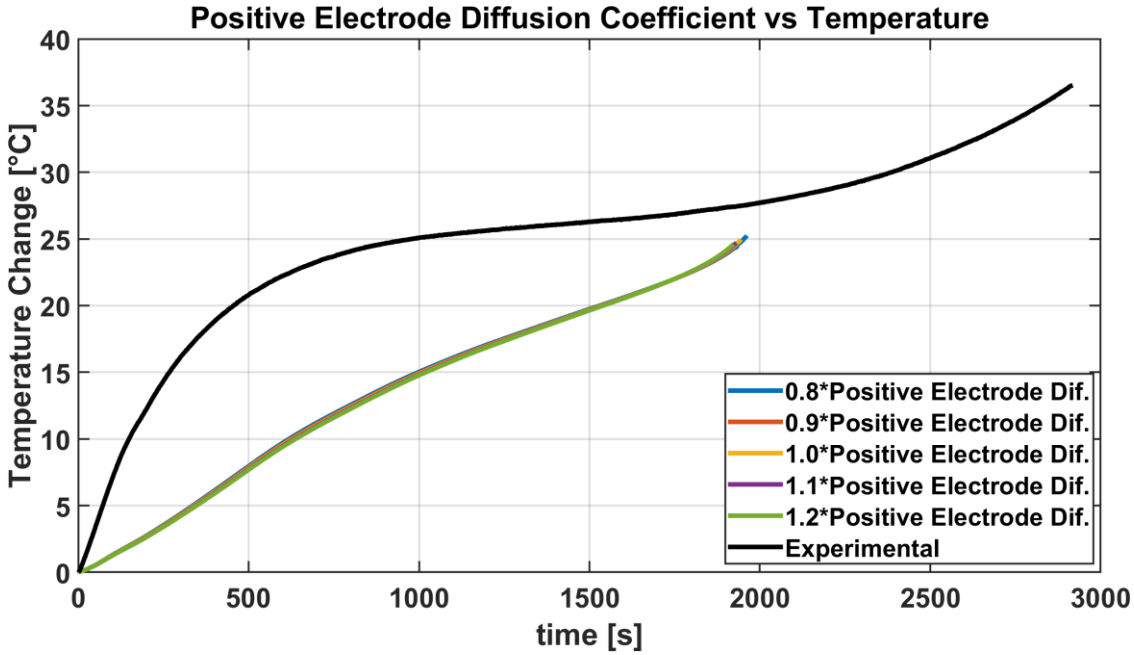

Figure 4.9. Positive Electrode Diffusion Coefficient vs Temperature

Decreasing positive electrode ionic diffusivity has little positive effect on voltage and temperature. Researchers reported ionic diffusivities around 1e-14 m^2/s for different cathode materials. In our simulations, the base model value starts

around 7e-15 m^2/s for the NCA cathode. It can be seen in Fig 4.6. and Fig. 4.8. that, changing the negative electrode diffusivity has more impact on the battery than changing the positive electrode diffusivity. In fact, studies suggest that poor performance of lithium-ion batteries at low temperatures, originates from sluggish anode diffusion [20, 67].

4.2.3. Electrolyte Diffusion Coefficient

Unlike electrodes, electrolytes do not have a porous matrix. Lithium ions can move freely across the electrolyte; thus, electrolytes have almost constant solvated lithium-ion concentration throughout operations. However, under high C-rates and low temperatures, higher lithium-ion concentration gradients occur in the electrolyte. For those reasons, electrolyte properties are represented with concentration and temperature dependent equations more accurately. The effect of changing lithium diffusivity in electrolyte is presented below in Fig 4.10. and Fig 4.11..

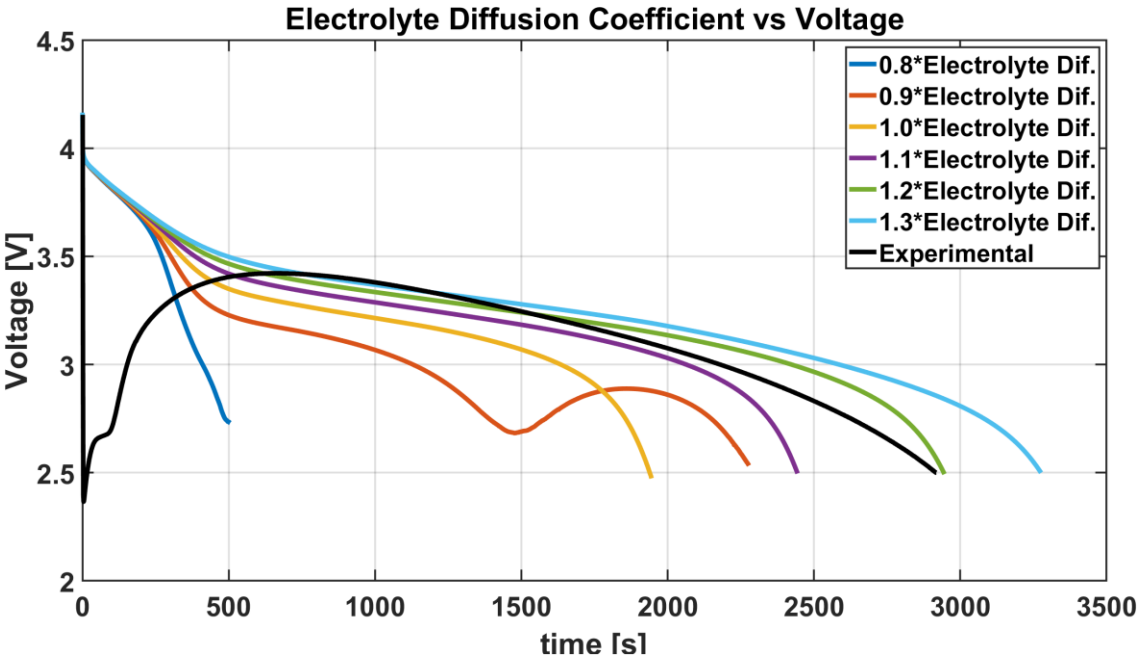

Figure 4.10. Electrolyte Diffusion Coefficient vs Voltage

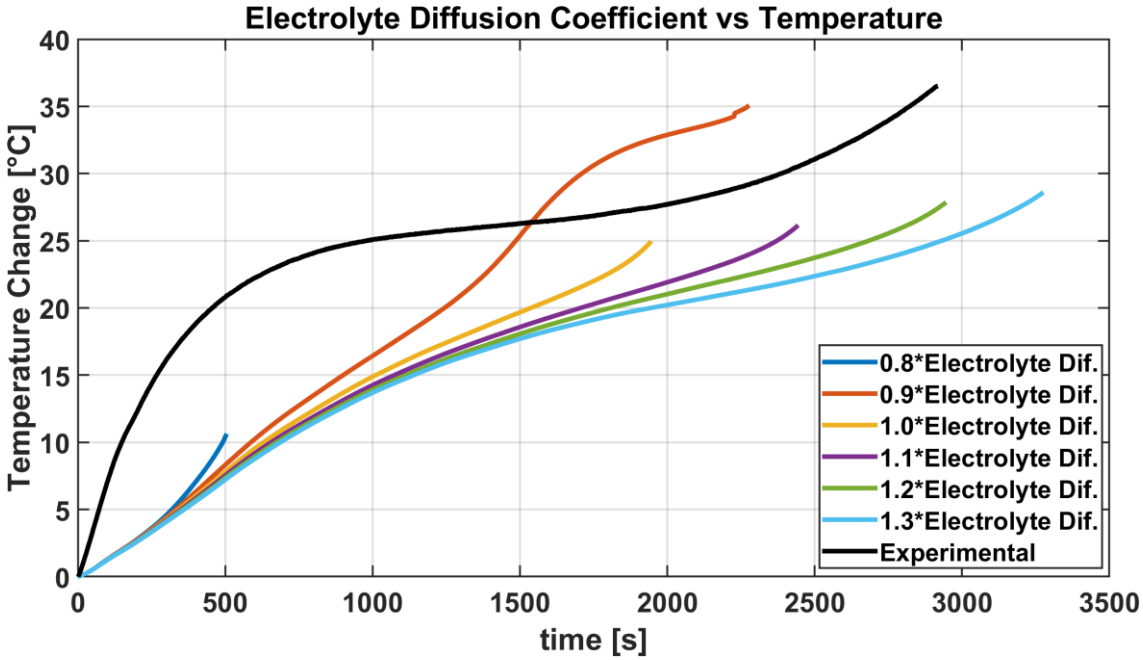

Figure 4.11. Electrolyte Diffusion Coefficient vs Temperature

One of the pronounced effects is obtained by modifying the electrolyte diffusion coefficient. The base model value starts from 1.16e-10 m^2/s and then rises with the temperature increase. Gallagher et al. [44] developed a phase-transition model for graphite electrodes also using 1.2M $LiPF_6$ in EC:EMC (3:7) electrolyte in experiments. They used a formulation that gives a value of 1.19e-11 m^2/s at -20°C for the electrolyte diffusion coefficient. However, equations in Table 2.4. and base model diffusion coefficient are generally obtained empirically without using any data at -20°C. There could be discrepancies at which the base model value is underestimated. That may be the reason why 90% and 80% of the base model value resulted in such unreasonable voltages.

Knowing that battery internal resistance increases at low temperatures, changing the diffusivity of the electrolyte has the most significant impact on battery internal resistance. This in return implies that electrolyte diffusivity is one of the leading causes of increased battery resistance.

4.2.4. Electrolyte Ionic Conductivity

Electrolyte conductivity was the first property that was thought to be the source of poor performance of lithium-ion batteries at low temperatures. Electrolyte conductivity refers to the charge conservation in the liquid phase. Fig 4.12. and Fig 4.13. show the results of changing electrolyte conductivity. It is clear that, despite being not effective as electrolyte diffusion, electrolyte conductivity is still important.

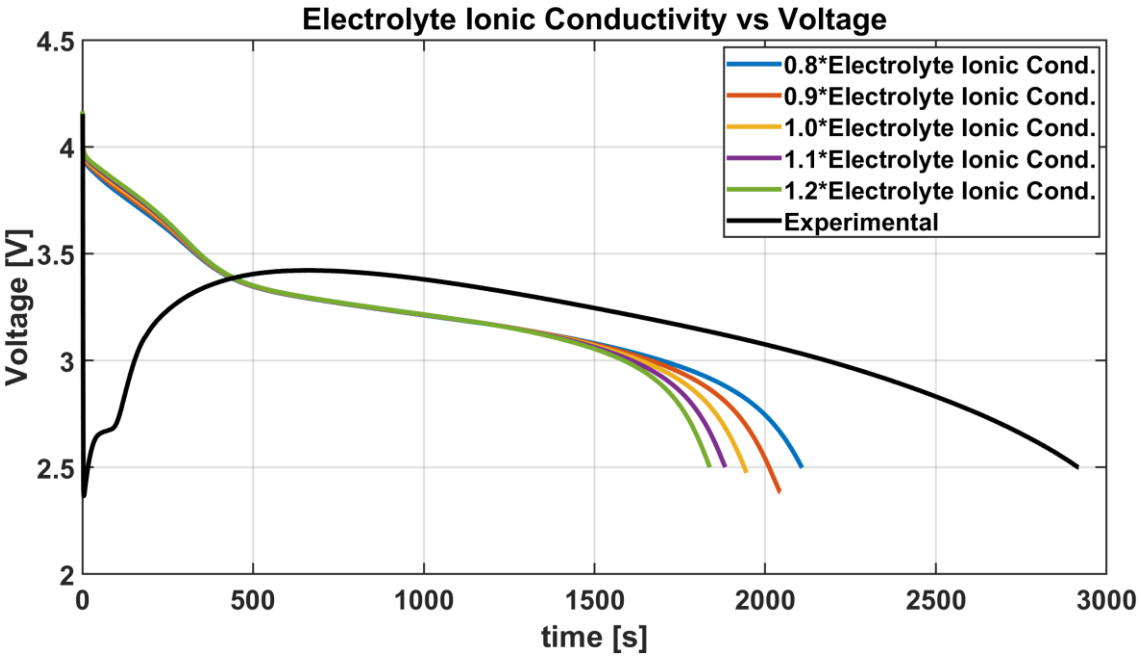

Figure 4.12. Electrolyte Ionic Conductivity vs Voltage

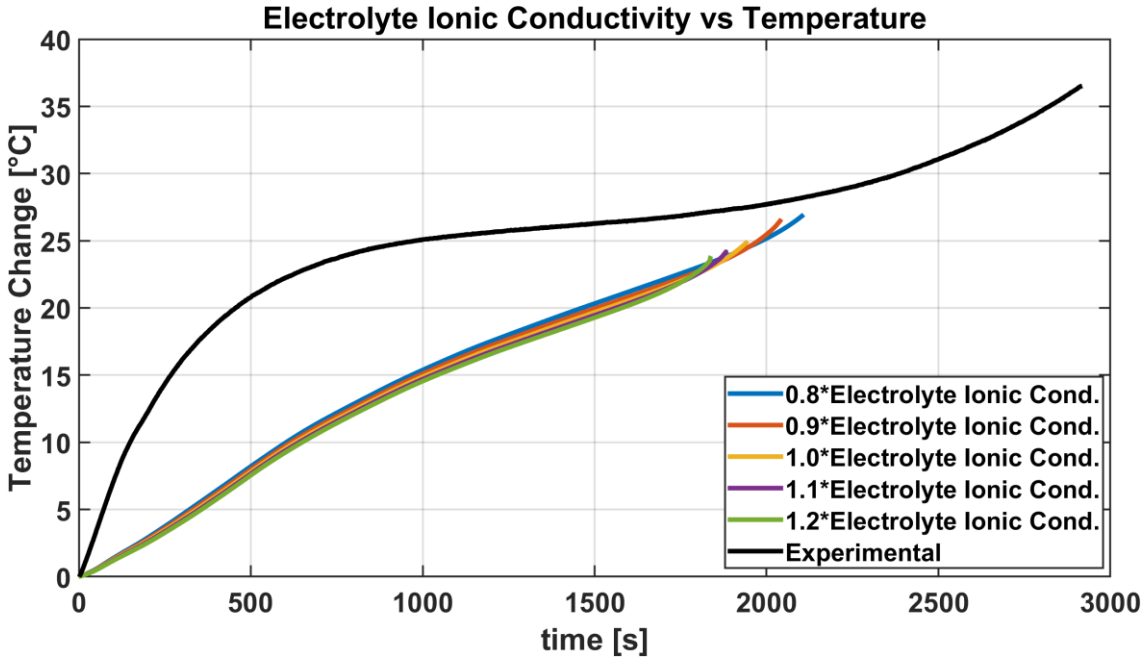

Figure 4.13. Electrolyte Ionic Conductivity vs Temperature

Decreasing electrolyte conductivity by 20% results in charged particles moving harder through the electrolyte, because of the decreased ionic mobility at low temperatures. Ionic mobility is a property that connects diffusivity and conductivity in electrolyte and is the estimation of how well the ions move through electrolyte under an electrical field or a concentration gradient. In both diffusion and ionic conduction, lithium ions move to a vacant position. But lower diffusivity leads to higher local concentration gradients, which in turn leads to lower conductivity. It's the reason why adjusting diffusivity in electrolyte results in more impact than changing conductivity.

4.2.5. Bruggeman Coefficients

The Bruggeman coefficient is one way of correcting electrochemical properties for porous structures such as electrodes and separators. In volume averaged modeling methods, it is needed to homogenize porous structures so that the structural differences can be represented without any need for complex modeling parameters. FIGURES show the effect of changing the positive electrode Bruggeman coefficient in simulations.

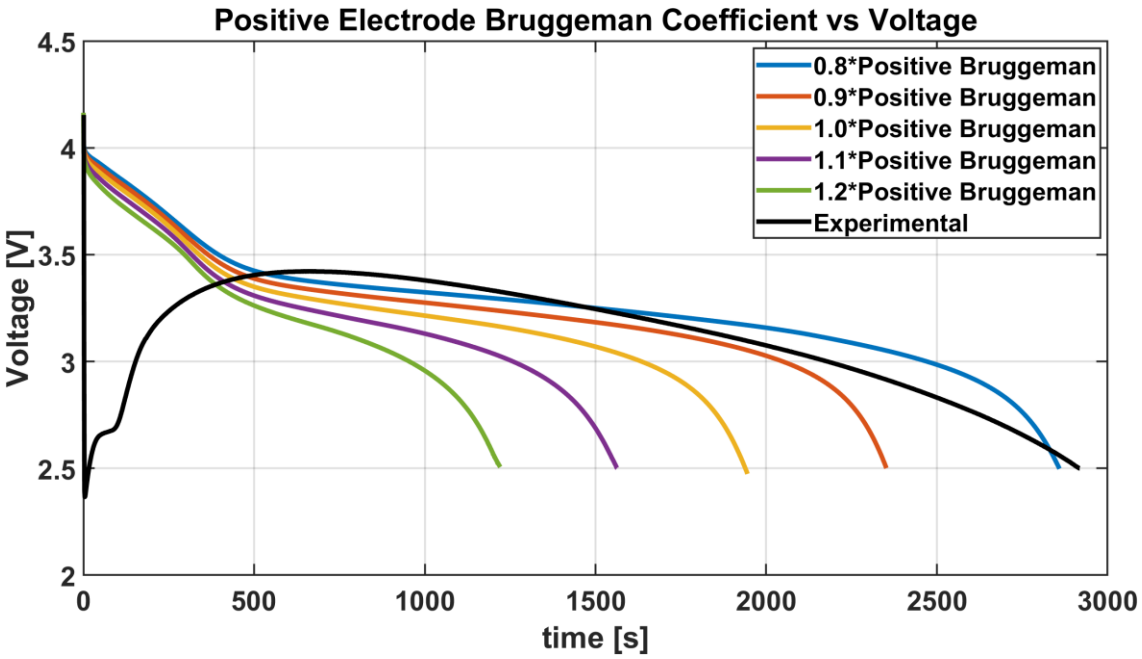

Figure 4.14. Positive Electrode Bruggeman Coefficient vs Voltage

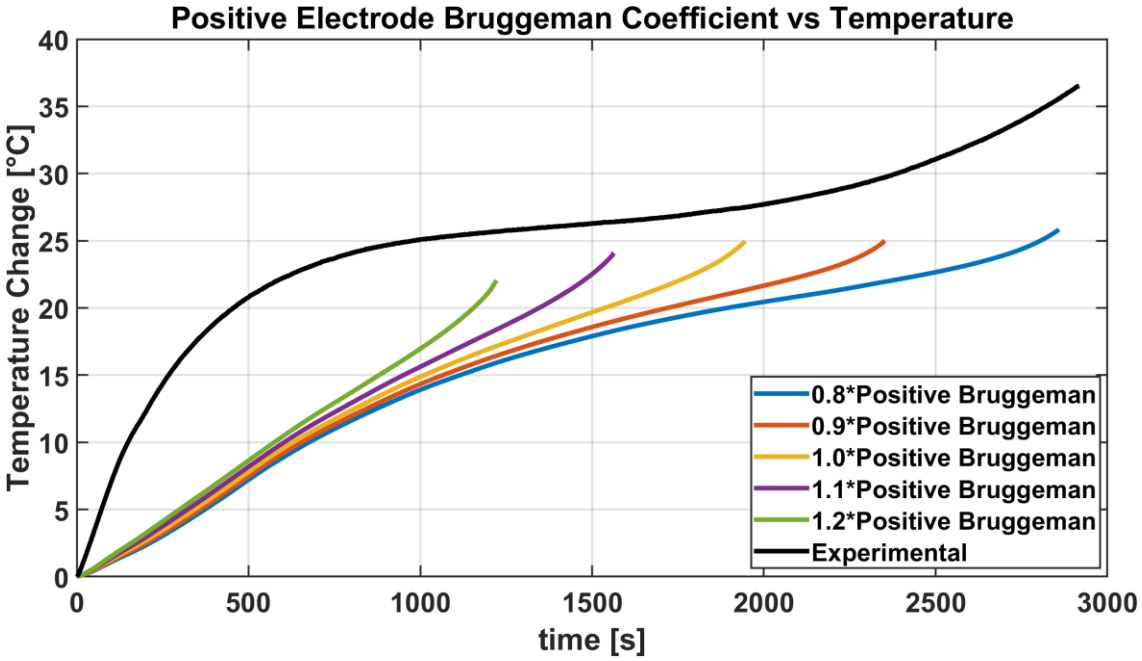

Figure 4.15. Positive Electrode Bruggeman Coefficient vs Temperature

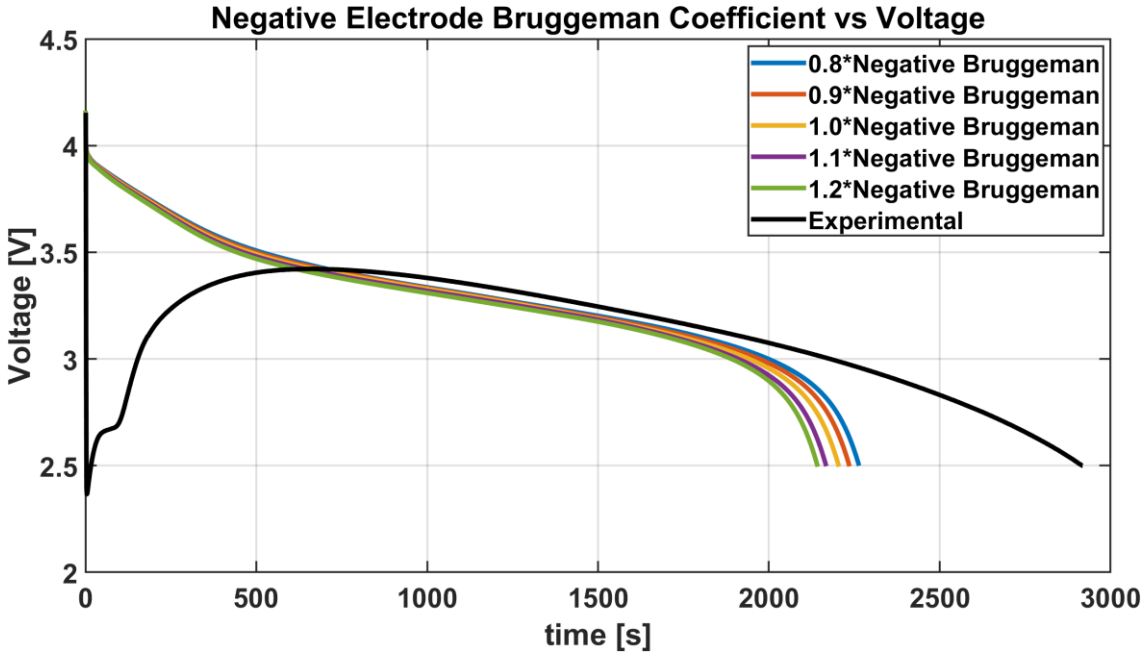

Figure 4.16. Negative Electrode Bruggeman Coefficient vs Voltage

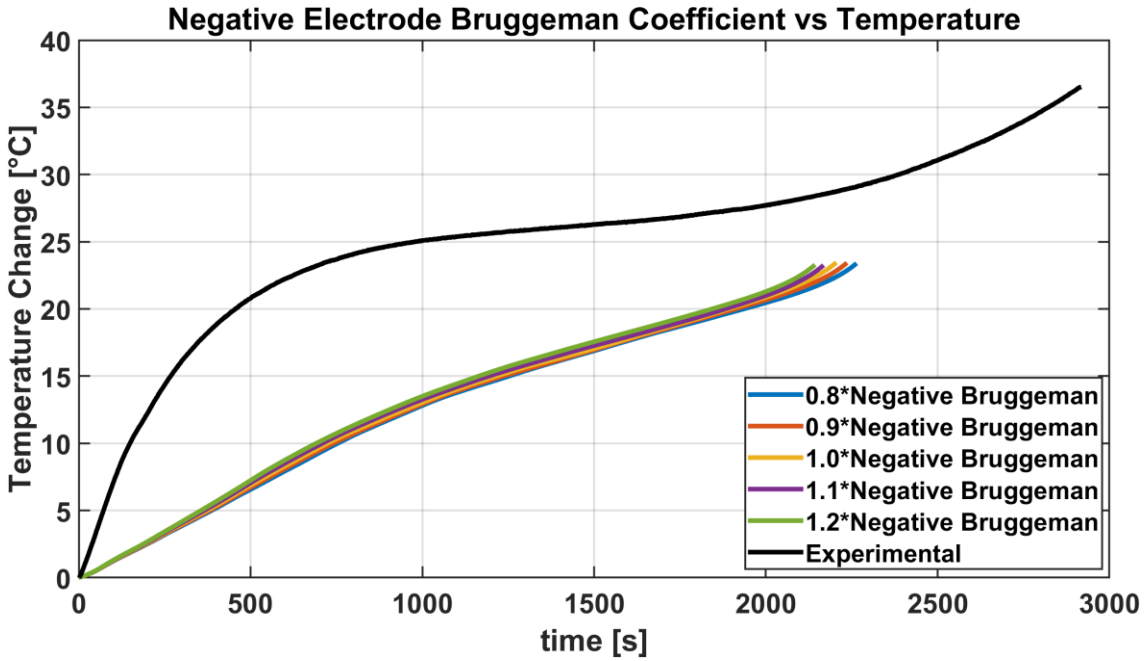

Figure 4.17. Negative Electrode Bruggeman Coefficient vs Temperature

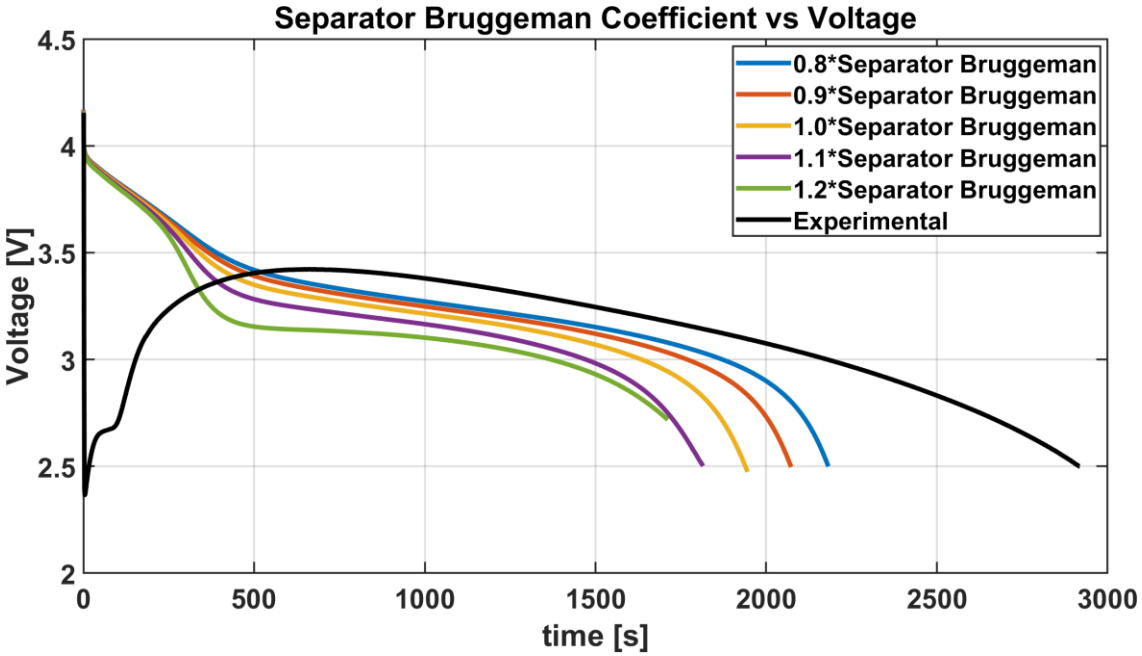

Figure 4.18. Separator Bruggeman Coefficient vs Voltage

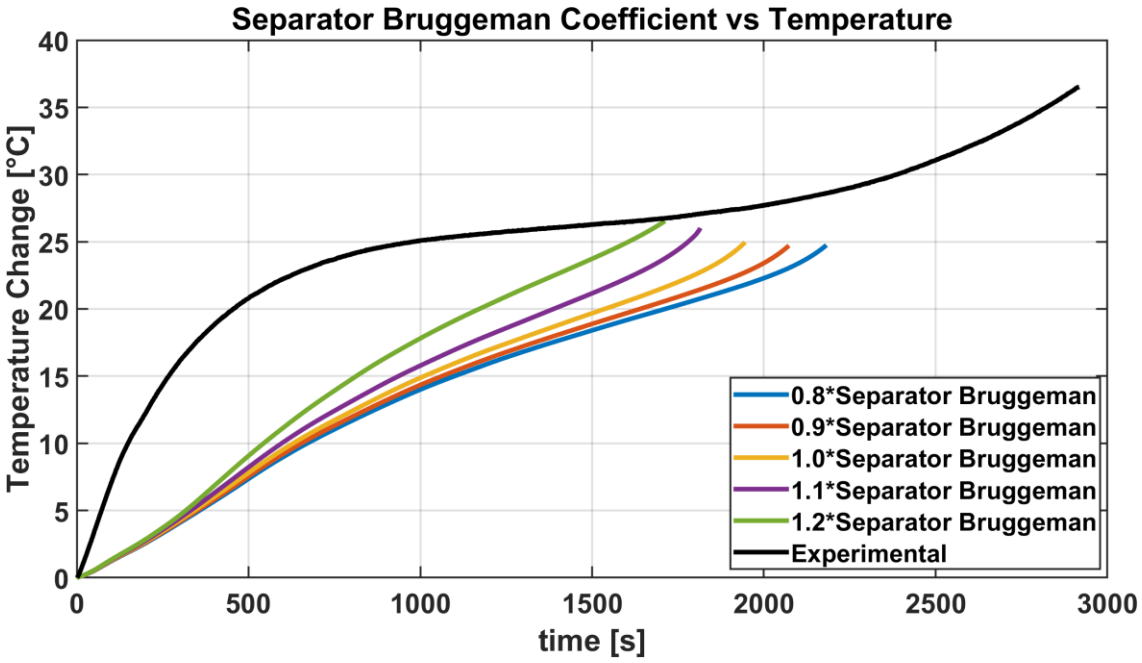

Figure 4.19. Separator Bruggeman Coefficient vs Temperature

Increasing the Bruggeman coefficient may account for larger tortuosity in the electrodes and the separator. Tortuosity is a property of porous materials such as electrodes and separators. It is defined as the ratio of the actual distance that is traveled by the fluid and the smallest distance between the flow path ends.

Larger tortuosities indicate that the lithium ions have to go through larger distances. Larger tortuosities, therefore, decrease the diffusion rate of the lithium ions, creating concentration gradients within the porous materials which reduces lithium-ion battery performance. Accordingly, in Fig 4.14 and Fig. 4.16., it can be seen that an increase in the Bruggeman coefficient decreased the discharge time. For the separator and positive electrode, base model values for the Bruggeman coefficients are 3.0 and 2.89 respectively, while the negative electrode Bruggeman coefficient is 1.5. Thus, modifying the negative electrode Bruggeman coefficient 10% at a time had less effect than the others.

Bruggeman coefficient is not exactly a parameter that has to be changed with the temperature, since the porosity and tortuosity do not change with the temperature. However, for the solid phase conduction, percolation of the non-conducting phase in the solid phase can reduce the electrical conduction as explained by Tagade et al. [53]. This percolation effect is affected by the temperature and can be captured by defining a temperature dependent Bruggeman coefficient.

4.2.6. Transport Number

Electrolyte transport number is a measure of mobility of the electrolyte ions, in this case ($LiPF_6$), Li^+, and PF_6^-. In lithium-ion batteries, Li^+ ion constitutes the charge transfer inside the battery. Therefore, all operations are dependent on lithium-ion mobility. For Li^+ ion, the transport number or transference number is represented by Eqn. (34),

$$t_+ = \frac{D_+}{D_+ + D_-} = \frac{\sigma_+}{\sigma_+ + \sigma_-} = \frac{\mu_+}{\mu_+ + \mu_-} \tag{34}$$

where, D is the diffusivity, σ is the conductivity, and μ is the mobility of the respective species, + for cation (Li^+) and – for anion (PF_6^-). The transport number represents the ratio of electric current carried by the cations to the total electric current. Fig 4.20. and Fig 4.21. show the effect of transport number on the battery performance.

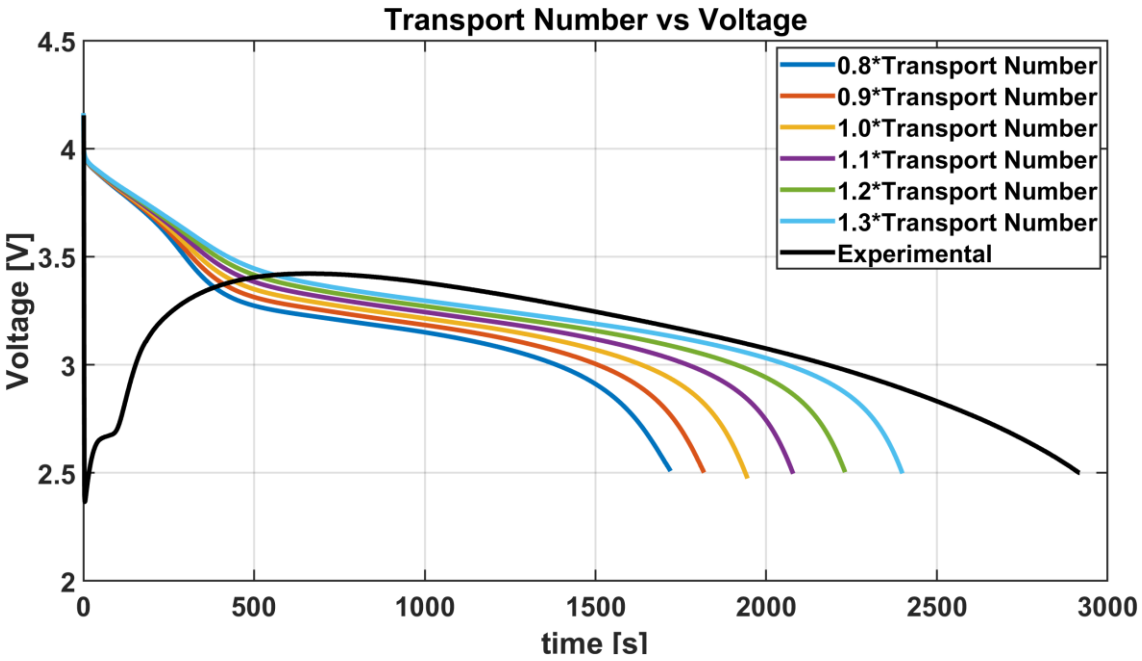

Figure 4.20. Electrolyte Transport Number vs Voltage

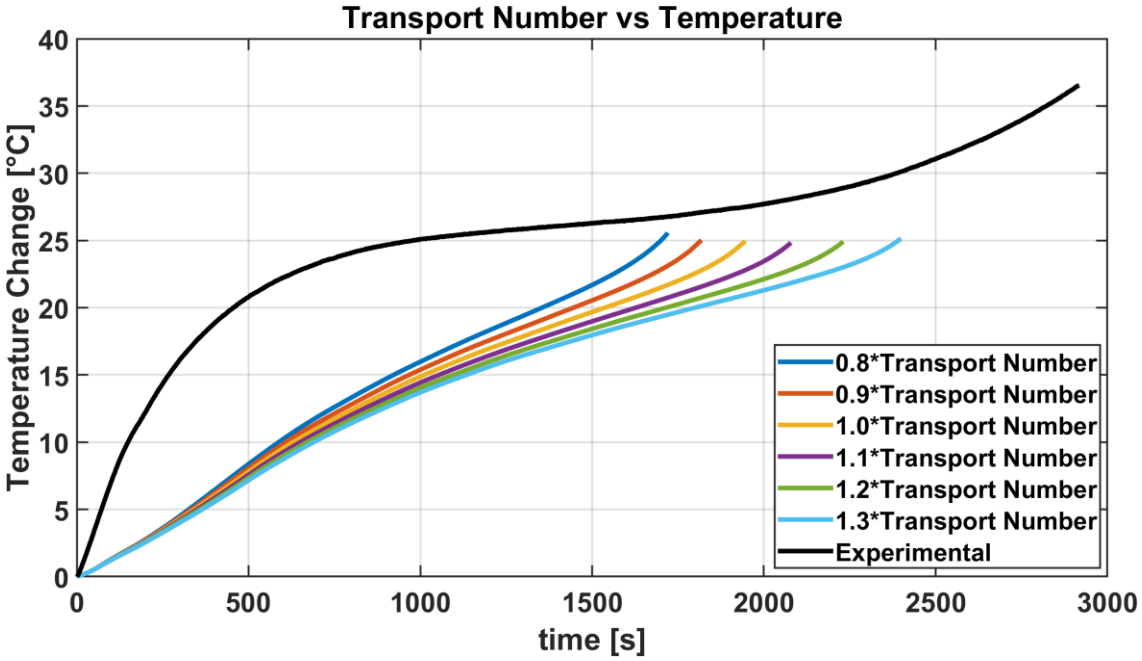

Figure 4.21. Electrolyte Transport Number vs Temperature

A larger transport number means that lithium ions move freely better. Therefore, it reduces concentration gradients in the electrolyte, creating less polarization. At

low temperatures, the transport number of cations obviously gets lower [45, 68], since the mobility is lower at low temperatures. However, the mobility of the lithium ions also depends on the solvent compound and lithium concentration in the electrolyte.

At -20°C temperature simulations, increasing transport number by 20% has increased the discharge time by 15%, while the temperature change attained at the end of the discharge remained almost the same. However, changing the transport number without changing at least the diffusivity of the electrolyte is not meaningful, since, it is a comparison of the diffusivity of the cation and the diffusivity of the total charged species in the electrolyte.

4.2.7. Activity Dependence ($\frac{\partial \ln f_{\pm}}{\partial \ln c_l}$)

Thermodynamic factor (TDF=1+$\frac{\partial \ln f_{\pm}}{\partial \ln c_l}$) is one of the transport properties of the electrolytes that are needed to be determined for capturing the right electrolyte behavior. It represents the non-ideal thermodynamic behavior of electrolytes. In an ideal electrolyte solution, the activity of the ions (activity coefficient) does not change with the concentration and the thermodynamic factor goes to 1.

In our simulations, $\frac{\partial \ln f_{\pm}}{\partial \ln c_l}$ is expressed in a function named “actdep_int1”. Changing this parameter would actually change “TDF-1”, but we can compare it with the trend of thermodynamic factors in the literature. Fig 4.22. and Fig 4.23. show the effect of changing activity dependence at low temperatures.

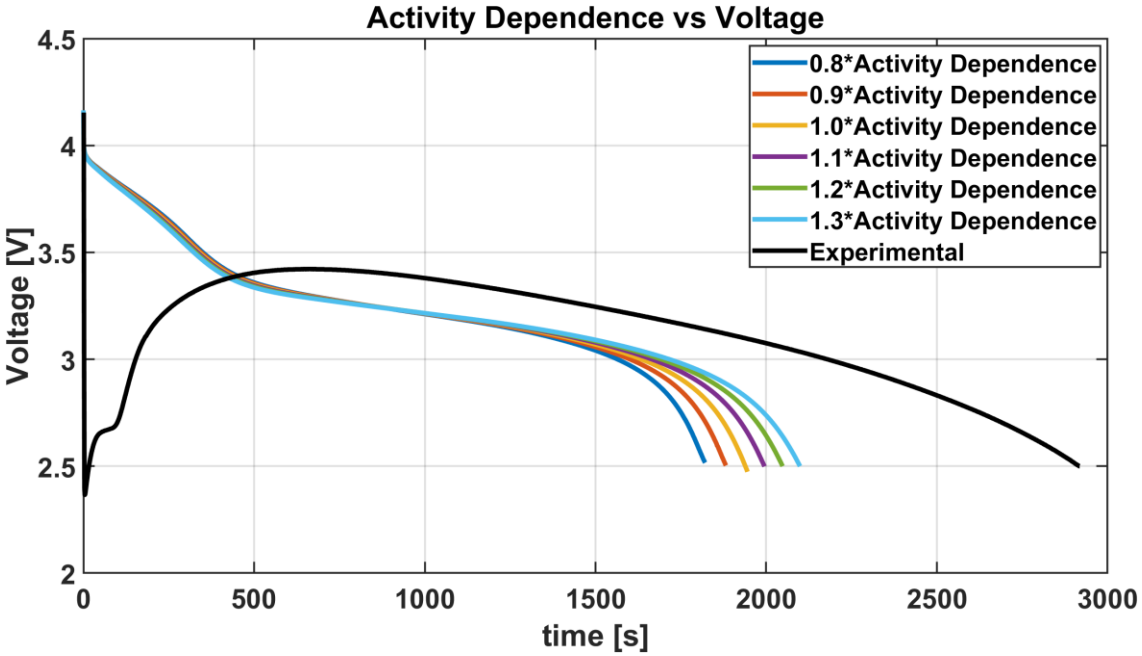

Figure 4.22. Electrolyte Activity Dependence vs Voltage

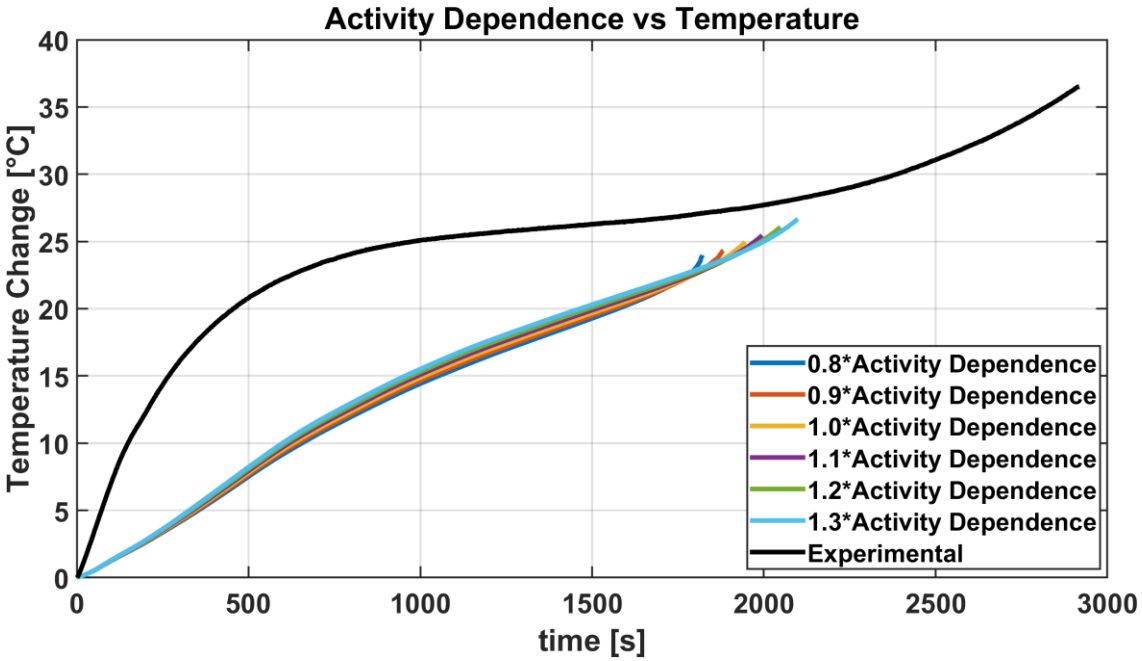

Figure 4.23. Electrolyte Activity Dependence vs Temperature

Activity dependence is affected by some factors such as ion-solvent and ion-ion interactions. Both interaction types affect the free energy of the solvated ions. As temperature decreases lithium ions in solvation shells are more tightly bound by the solvents. Therefore, the activity coefficient of the ions decreases hence the

activity dependence gets low. This could potentially make a solution to act more ideally (TDF=1). However, at the same time, the necessary energy to desolvate lithium ions at the interface of the electrode and electrolyte becomes greater.

In the simulations, lowering the activity dependence value decreased the discharge time as it decreases the effective concentrations of ions, therefore decreasing the movement of the species. 20% decrease in activity dependence decreased the discharge time by 6%, delivering lower capacity, as expected from a lithium-ion battery at low temperatures.

4.2.8. Reaction Rate Constants

Reaction rate constants represent the speed of the lithium insertion and extraction reactions at the electrodes. In Eqn. (28) and Eqn. (29), it can be seen that for a constant volumetric reaction rate J_i, lowering reaction rate constants cause higher overpotential values. Therefore, it could be suggested that low reaction rate constants contribute to the charge transfer resistance.

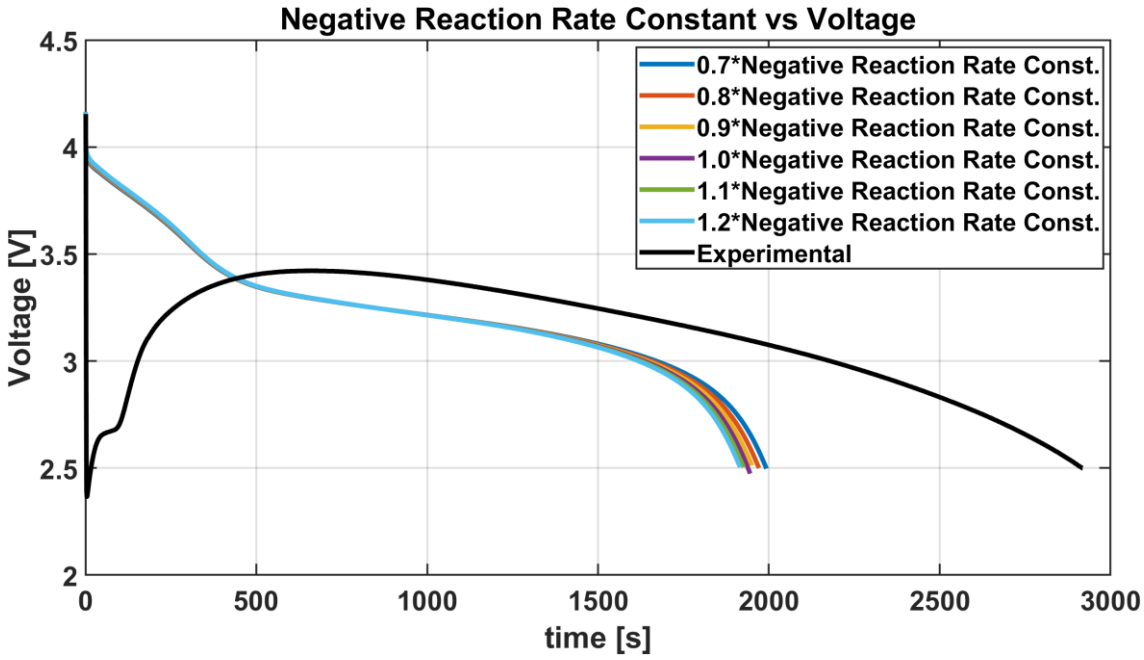

Figure 4.24. Negative Electrode Reaction Rate Constant vs Voltage

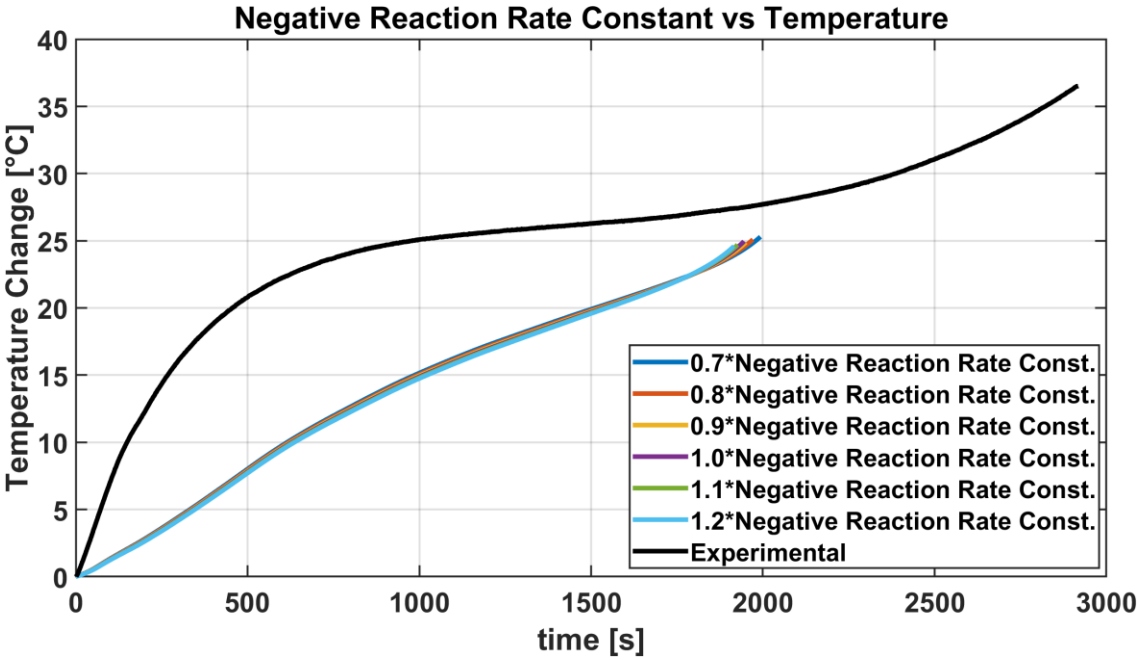

Figure 4.25. Negative Electrode Reaction Rate Constant vs Temperature

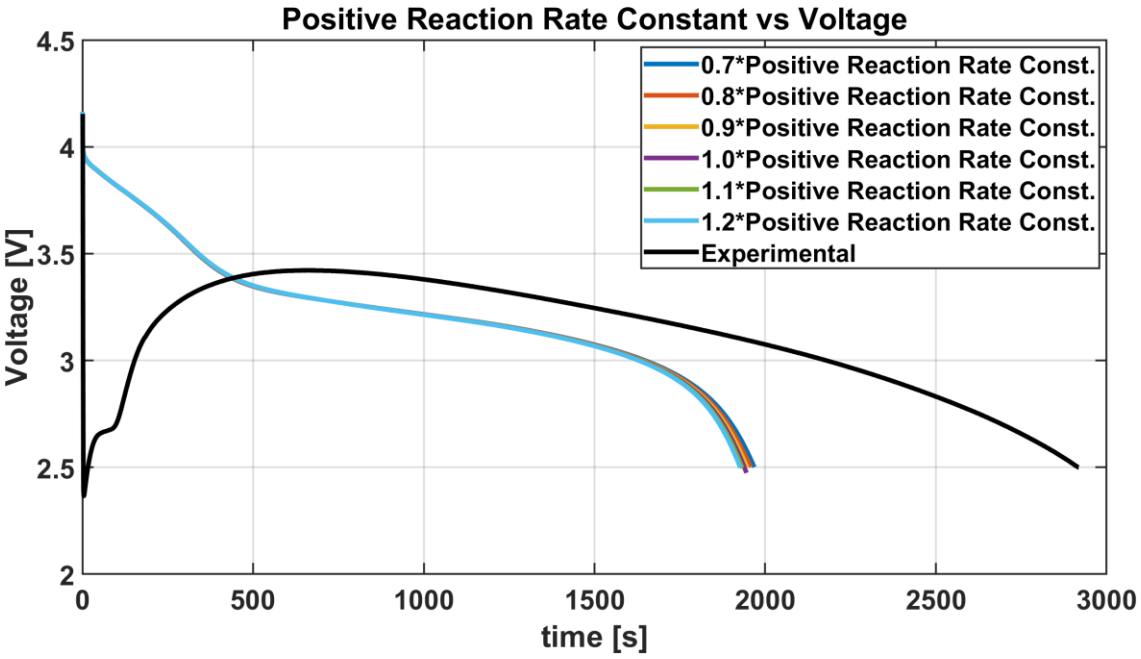

Figure 4.26. Positive Electrode Reaction Rate Constant vs Voltage

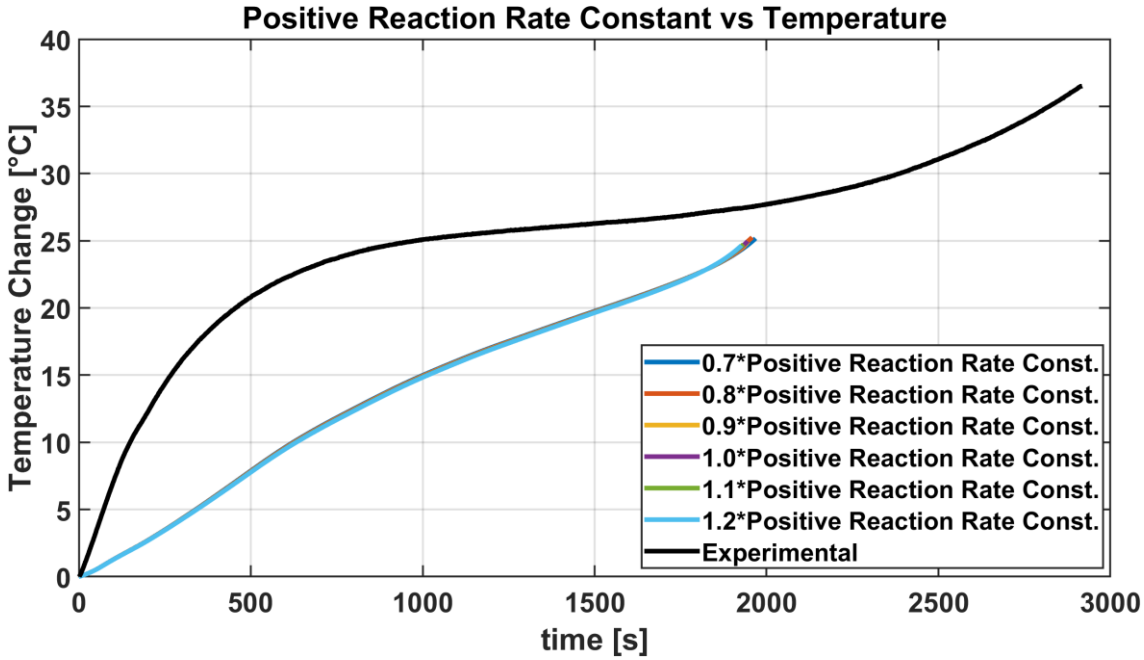

Figure 4.27. Positive Electrode Reaction Rate Constant vs Temperature

Fig 4.24., Fig. 4.25., Fig. 4.26., Fig. 4.27. show the effect of changing reaction rate constants on the battery voltage and temperature. It can be seen from the RMSE values, changing the negative electrode value has a more pronounced effect on the battery than changing the positive electrode value. That is in agreement with the low temperature performance studies [1, 18, 24, 65]. In the FIGURES additional 70% of reaction rate constant data are shown to better observe the effects of decreased reaction rate constants. In both electrodes, a lower reaction rate constant decreased the RMSE value since it creates a larger overpotential, and decreasing the temperature has the same effect on overpotential.

4.2.9. Specific Heat Capacity of the Battery

Specific heat capacity is another property that can change with respect to temperature. It is defined as the amount of heat necessary to increase the temperature of the unit mass of the battery. While specific heat capacity seems to be an entirely thermal parameter, it is also affected by the battery SOC [69]. In our simulations, the base model value for the specific heat capacity of the battery

is taken from [70], which is 750 J/kg.K. Fig 4.28. and Fig 4.29. below, show the results of different battery specific heat capacities in simulations.

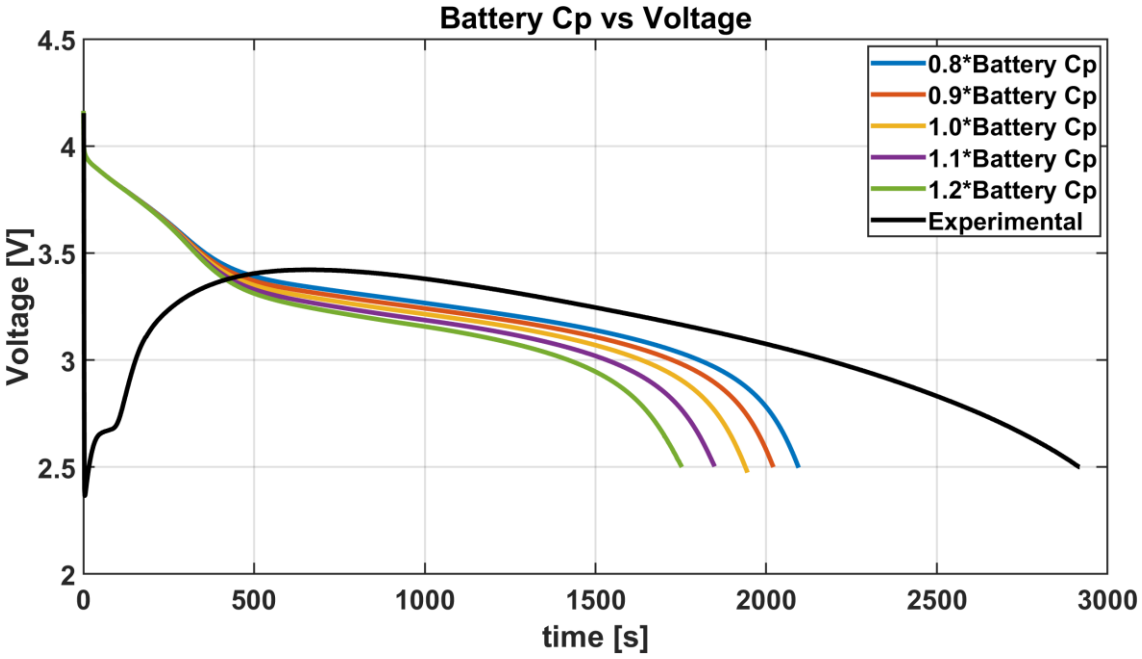

Figure 4.28. Battery Specific Heat Capacity vs Voltage

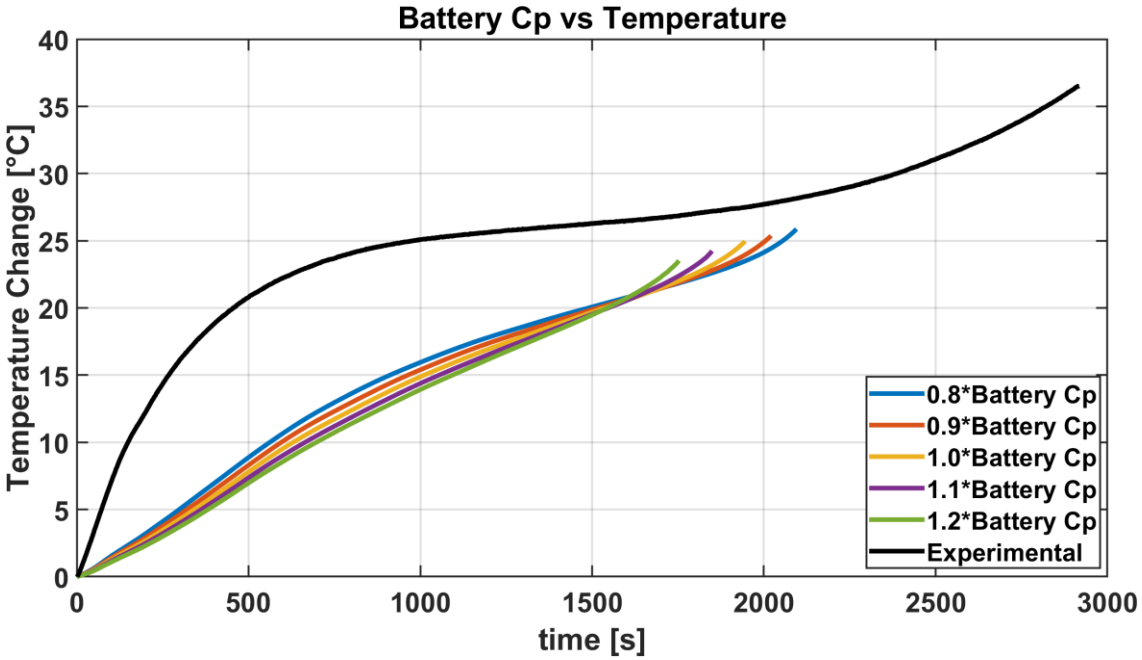

Figure 4.29. Battery Specific Heat Capacity vs Temperature

At the very start, battery voltages do not vary for different C_p values, creating same overpotentials, while the temperature differences can be seen right after initiation. This could mean that the heat generation is around the same for all C_p values at the start. However, as the differences in the temperature increasing rates become more noticeable, the electrochemical properties of the battery begin to change in a separate manner. After a while, these changes in electrochemical properties produce dissimilar overpotentials. Looking at the total discharge, it can be argued that the batteries whose temperatures can be increased more easily should perform better at low temperatures. 80% of the base model C_p generated nearly 10% more discharge time and decreased the RMSE values remarkably.

4.2.10. SEI Film Resistance

Solid electrolyte interphase (SEI) is usually used for naming the film formed at the anode-electrolyte interface. It begins to form from the start of the first cycling operation and continues to develop slowly as the cycling number increases. The building blocks of the SEI layer are the electrolyte solvents and the lithium salts in the battery. During the first operation, the electrolyte reacts with the anode and decomposes into a thin film on the anode surface. As the layer grows, it does not allow electrons to move past it and stops the growth of the SEI layer. Therefore, it contradicts itself and disrupts the reduction of electrolyte further. In this manner, the SEI layer is needed for the safety and stability of the battery.

However, as the SEI layer grows thicker, the amount of cyclable lithium in the battery reduces, thus the reversible capacity decreases. Consequently, the resistance of the battery increases as it grows. Like the charge transfer resistance, SEI resistance is also highly temperature dependent [26]. In our simulations, the base model value for SEI resistance is zero. But for investigating the effect of SEI resistance on the battery performance and its temperature dependence, a value from the literature, which uses the same battery Panasonic NCR18650B, is used [71]. While it is more than just SEI resistance according to the authors, it will be a useful starting point for numerically investigating the

effects of temperature dependent SEI resistance on the battery. Eqn. (35) below represents the SEI resistance used in this study,

$$R_{SEI} = \frac{0.2978426}{1 + 0.17335(T - 253.15)} \tag{35}$$

where T is the battery temperature. Effect of carrying film resistance on the battery is shown below in Fig. 4.30. and Fig. 4.31..

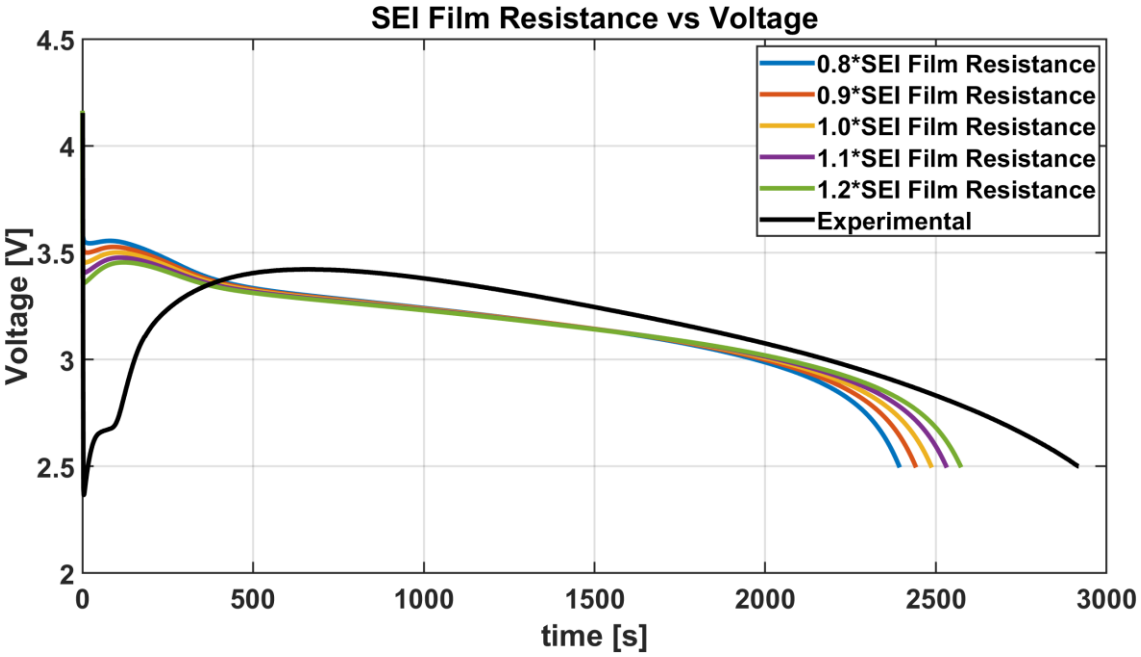

Figure 4.30. SEI Film Resistance vs Voltage

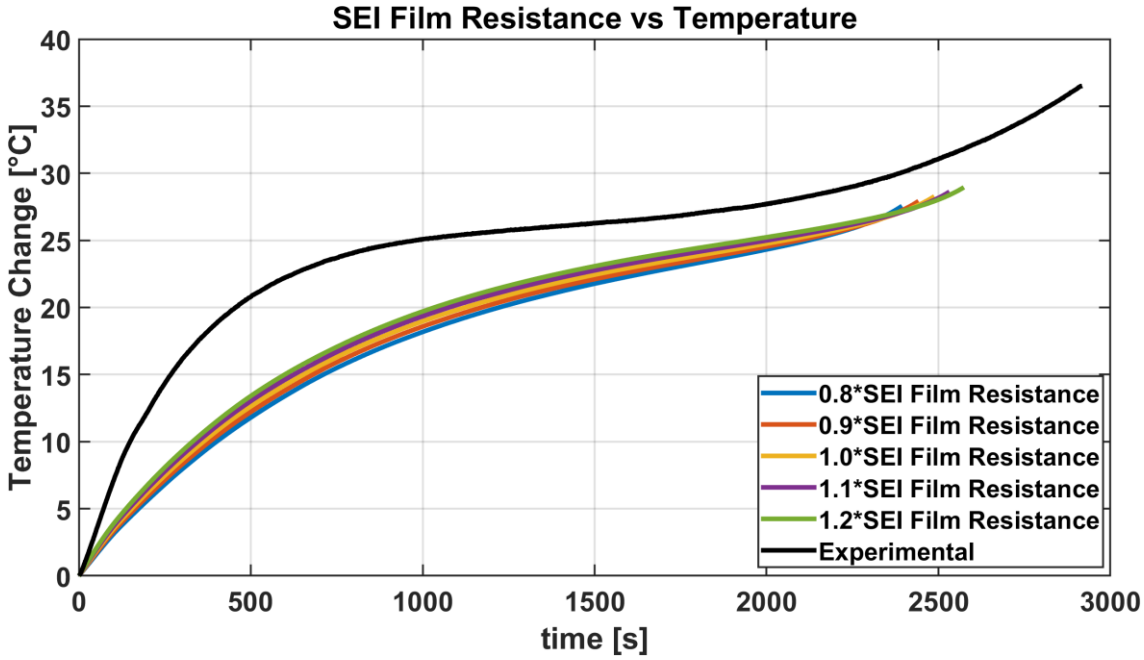

Figure 4.31. SEI Film Resistance vs Temperature

Out of all the varied parameters, SEI resistance had the most dramatic effect on the battery. One of the largest overpotential effects at the start of the simulation occurred just by inserting Eqn. (35) into the model. Starting voltage dropped from 3.9V to 3.5V when the SEI resistance term was added. SEI resistance term stretched the discharge time 500 seconds.

At the start of the discharge, voltage rebound is began to be seen more clearly. This effect which is the most realistic case at -20°C ambient temperature was not attained by changing other battery parameters. The voltage rebound occurs as a result of self-heating. Increased resistances at low temperatures cause higher ohmic heat generation which in turn causes the battery to recover a little. Increasing SEI resistance further proved to generate more heat, inducing higher degrees of recoveries.

4.3. Combined Effects of Two Influential Parameters

In this part of the study, two of the most influential parameters are combined. The SEI resistance and the positive electrode Bruggeman coefficient are varied

together. RMSE values are calculated as can be seen in Table 4.3. and Table 4.4. and the best fit is shown in Fig. 4.32. and Fig. 4.33.

Table 4.3. RMSE Values of SEI Resistance and Positive Electrode Bruggeman Coefficient vs. Voltage.

		$brugg_{pe}$				
	%Percentage	**80**	**90**	**100**	**110**	**120**
R_{SEI}	**100**	0.2442	0.2147	0.2355	0.2975	0.3643
	150	0.2125	0.1936	0.1909	0.2567	0.3318
	200	0.1854	0.1731	0.1645	0.2296	0.3131
	250	0.1646	0.1582	0.1555	0.2136	0.3041
	300	0.152	0.1515	0.1578	0.2086	0.3028

Table 4.4. RMSE Values of SEI Resistance and Positive Electrode Bruggeman Coefficient vs. Temperature.

		$brugg_{pe}$				
	%Percentage	**80**	**90**	**100**	**110**	**120**
R_{SEI}	**100**	7.2262	6.1897	5.2819	5.0262	4.9118
	150	6.0353	5.0504	3.8248	3.4983	3.4967
	200	4.9067	4.002	2.7597	2.4136	2.7795
	250	3.8646	3.0573	2.0324	1.9248	2.8491
	300	3.2984	2.5701	1.7257	1.9782	3.181

Similar to the previous SEI resistance study, increasing SEI resistance generally has a positive effect on the RMSE values. For the positive electrode Bruggeman coefficient, values around the base model result in better RMSE values, sometimes 90% is better, and sometimes 110% is better. Fig. 4.32. and Fig. 4.33. show the voltage and the temperature estimation for 300% SEI resistance with varying positive electrode Bruggeman coefficient.

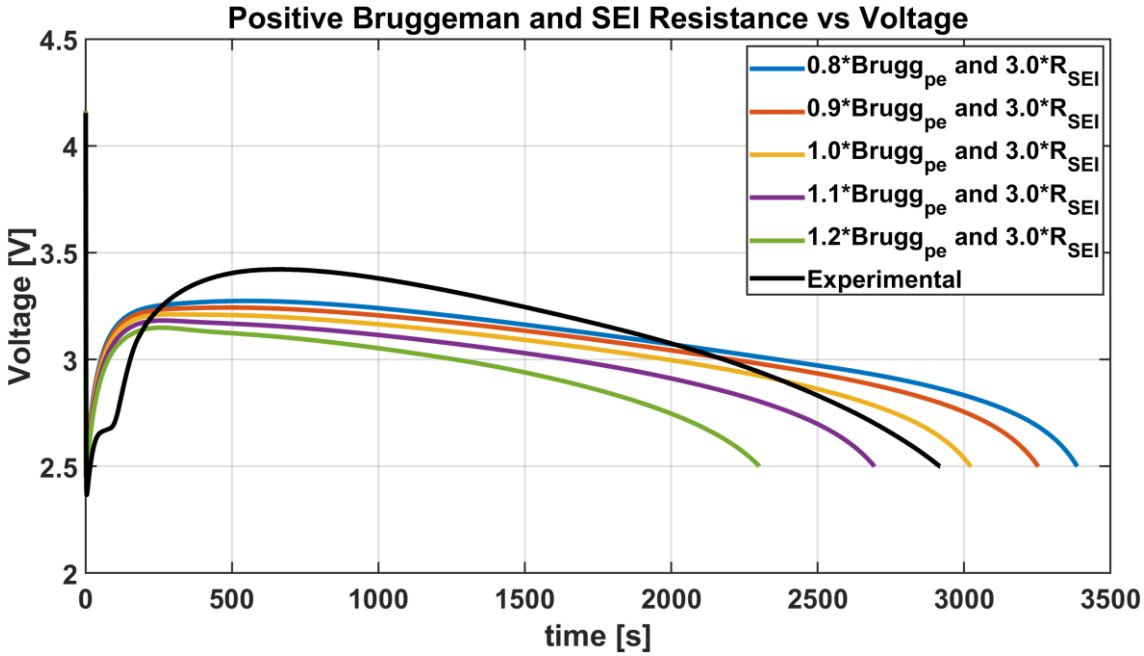

Figure 4.32. 300% SEI Resistance and Varying Positive Electrode Bruggeman Coefficient vs Voltage

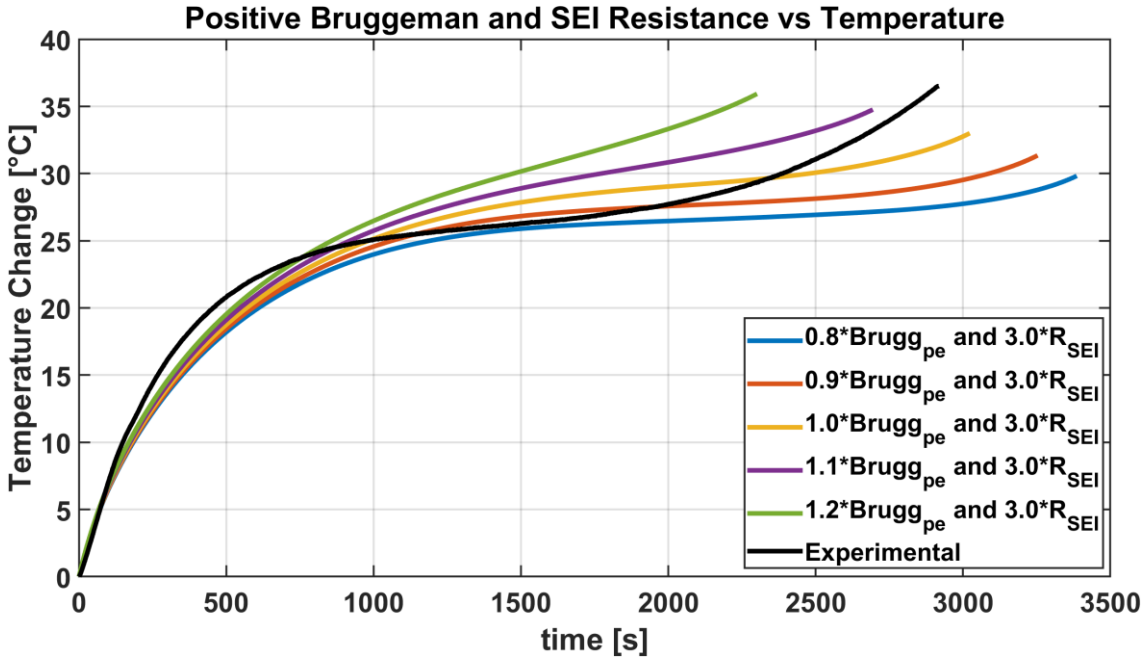

Figure 4.33. 300% SEI Resistance and Varying Positive Electrode Bruggeman Coefficient vs Temperature

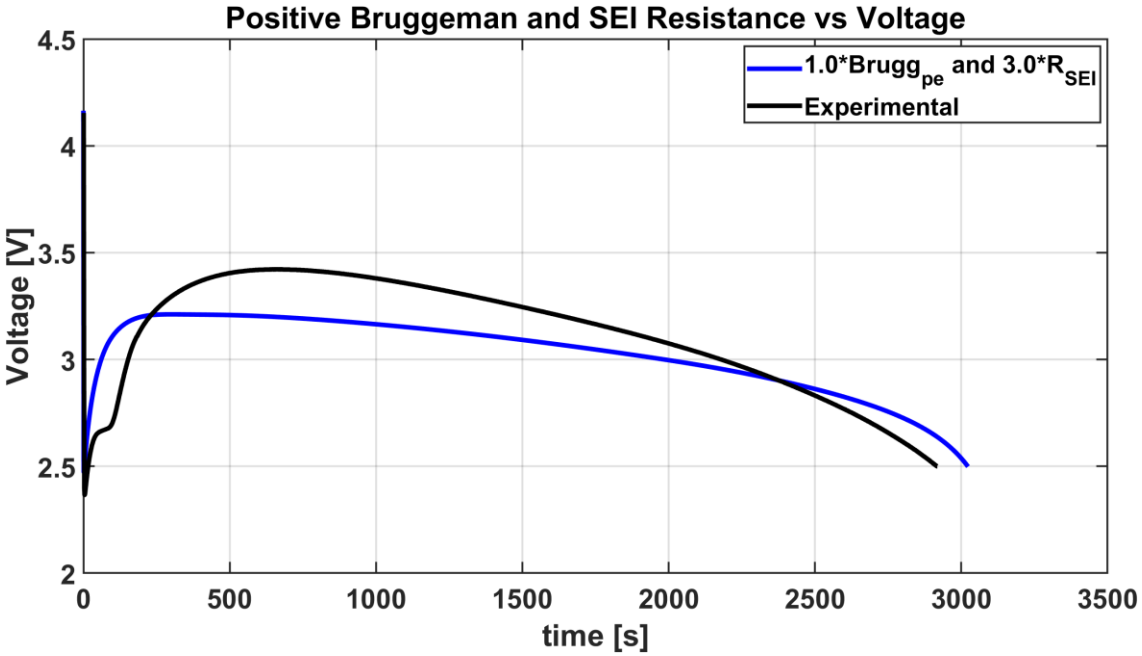

Figure 4.34. 300% SEI Resistance and 100% Positive Electrode Bruggeman Coefficient vs. Voltage

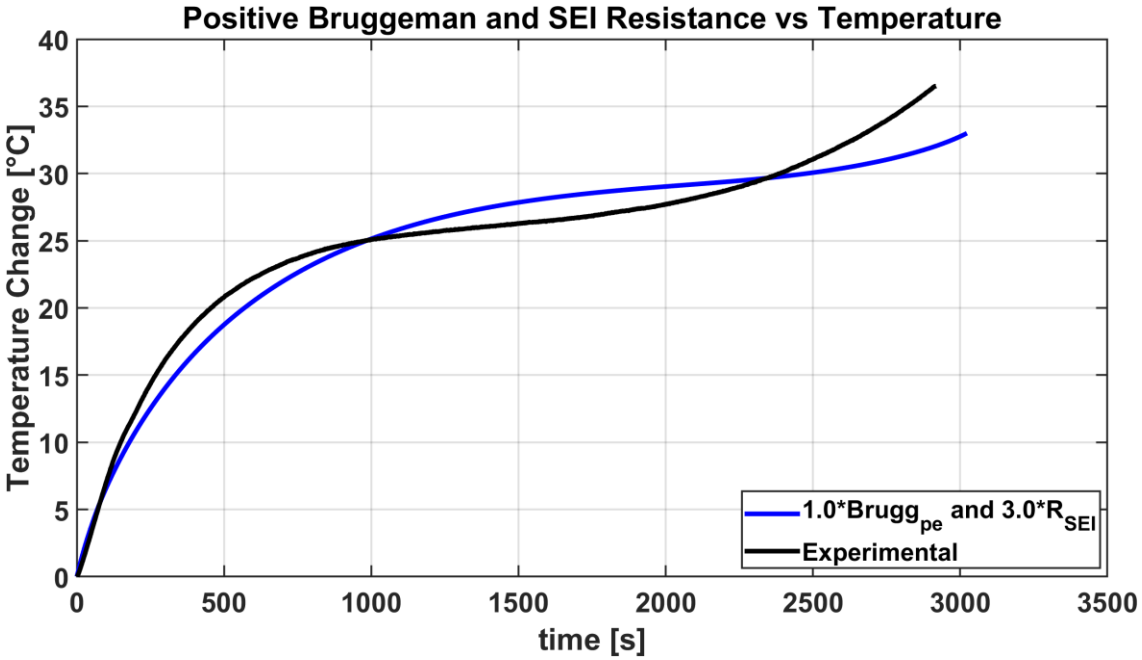

Figure 4.35. 300% SEI Resistance and 100% Positive Electrode Bruggeman Coefficient vs. Temperature

It can be seen that just by increasing SEI resistance further than the previous study, model accuracy increases significantly. With the addition of SEI

resistance, the positive electrode Bruggeman coefficient has less effect on discharge time than before. However, it also changes the maximum voltage attained after the voltage bounce.

After the voltage bounce, the model acts more linearly than the experimental data. After the horizontal temperature plateau, this linearity causes the temperature to rise later than the experimental data. While increasing the positive electrode Bruggeman coefficient decreases the temperature RMSE values, it increases the voltage RMSE values. Therefore, in Fig. 4.34. and Fig. 4.35., it is chosen to be 100% of the base model value as an example.

In Appendix 1, a similar study of combining the rest of the parameters can be found.

5. CONCLUSIONS

5.1. Conclusions

Energy storage systems are developing day by day. Increasing power and energy demand has made batteries a critical part of the world. As the options of renewable energies and capabilities are growing, batteries have become irreplaceable. Offering a high energy density among the batteries, lithium-ion batteries became the most preferred means of energy storage. Their aspects even proved to be useful for harsh environmental conditions such as space missions, various extreme ambient temperatures, and high-performance machines.

One of the greatest challenges in lithium-ion batteries is operations at low temperatures. Low temperatures have great impacts on lithium-ion battery performance, thermal behavior, cycle life, and safety. In order to understand such effects and safely perform operations at low temperatures, a comprehensive modeling effort is needed.

In this thesis, the performance and thermal behavior of a commercial lithium-ion battery were investigated at low temperatures. Identical batteries are subjected to 0.5C and 1.0C charge-discharge at three different temperature settings.

Conducted experiments showed that as the temperature decreases, the available capacity of the lithium-ion batteries decreases, and heat generation inside the battery increases. The performance of batteries becomes harder to predict since the electrochemical components suffer incredibly from their ideal capabilities. It is thought that lithium diffusion in both the solid and liquid phases reduces, losing the ability to intercalate/deintercalate in the solid phase and mobility in the liquid phase, therefore creating large concentration gradients that cause increased battery resistance as a result. Ionic conduction in the liquid phase decreases, resulting in a need for a higher driving force to move ions in the electrolyte and causing the rate capability of the lithium-ion battery to drop. The activity and the

mobility of the ions in the electrolyte decrease as the temperature gets lower. Resistances such as charge transfer resistance, and SEI resistance at bulk resistance of the battery increase, as a result, heat generation inside the battery increases, creating faster temperature rise and higher overall temperature which consecutively changes the electrochemical properties of the battery. Therefore, low temperature operations are a big challenge for battery thermal management systems.

As a part of this thesis, an available in-house electrochemical-thermal coupled model was employed to numerically investigate the effects of the varying model parameters at low temperatures. A few selected electrochemical parameters that were thought to be temperature dependent were changed one at a time between 80%-130% of their base model values for studying their effects on the battery performance and thermal behavior individually. Results are evaluated by calculating the root-mean-square error of the voltage and temperature simulations for each changed parameter. Results suggest that electrolyte properties such as ionic diffusion, conduction, transport number, and activity dependence play a big role in the battery performance and thermal behavior. Bruggeman coefficients of the porous components can be employed as temperature dependent in order to fit experimental results, as it is done in the literature for the other parameters frequently. Incorporating SEI film resistance into the model is crucial for estimating the battery voltage and temperature, as it was deduced to be the most important contributor to the overpotential at the start of the simulation and to the temperature rise.

In conclusion, battery simulations suggest that concentration dependence of the electrochemical properties might not reflect the actual behavior of the parameters and including temperature dependent characterization of the electrochemical properties is key to safe battery operations.

5.2. Recommendations for Future Work

Research can be expanded based on the results presented in this thesis. Effects of varying properties of battery casing materials and current collectors can be investigated at low temperatures. Thermal parameters corresponding to different insulation and ambient arrangements, such as thermal conduction coefficient and convection coefficient, and emissivity can be analyzed similarly.

The presented results can be compared only with the batteries that show negligible cycling capacity fade. The effects of varying model parameters on the cycling capacity fade can be investigated at low temperatures. For example, changing SEI thickness and properties can be implemented on the model.

Battery thermal management systems are designed for keeping the batteries at their optimal limits of operation. The sensitivity analysis results presented in this thesis can be an example for defining the requirements of battery thermal management systems when some of the battery electrochemical properties are unknown at low temperatures.

Finally, the effects of varying model parameters can be investigated on the charge characteristics of the battery.

6. REFERENCES

[1] T. R. Jow, S. A. Delp, J. L. Allen, J.-P. Jones, and M. C. Smart, "Factors limiting Li+ charge transfer kinetics in Li-ion batteries," *Journal of the electrochemical society,* vol. 165, no. 2, p. A361, 2018.

[2] D. Linden and T. B. Reddy, *Handbook of batteries*, 3rd ed. (McGraw-Hill handbooks). New York: McGraw-Hill, 2002.

[3] D. Bernardi, E. Pawlikowski, and J. Newman, "A general energy balance for battery systems," *Journal of the electrochemical society,* vol. 132, no. 1, p. 5, 1985.

[4] S. Chen, C. Wan, and Y. Wang, "Thermal analysis of lithium-ion batteries," *Journal of power sources,* vol. 140, no. 1, pp. 111-124, 2005.

[5] T. Özdemir, Ö. Ekici, and M. Köksal, "Numerical and experimental investigation of the thermal and electrical characteristics of a lithium ion cell," in *E3S Web of Conferences*, 2021, vol. 321: EDP Sciences, p. 03007.

[6] E. Gümüşsu, Ö. Ekici, and M. Köksal, "3-D CFD modeling and experimental testing of thermal behavior of a Li-Ion battery," *Applied Thermal Engineering,* vol. 120, pp. 484-495, 2017.

[7] H. Wu, X. Zhang, R. Cao, and C. Yang, "An investigation on electrical and thermal characteristics of cylindrical lithium-ion batteries at low temperatures," *Energy,* vol. 225, p. 120223, 2021.

[8] G. Karimi and X. Li, "Thermal management of lithium-ion batteries for electric vehicles," *International Journal of Energy Research,* vol. 37, no. 1, pp. 13-24, 2013.

[9] D. H. Jeon and S. M. Baek, "Thermal modeling of cylindrical lithium ion battery during discharge cycle," *Energy Conversion and Management,* vol. 52, no. 8-9, pp. 2973-2981, 2011.

[10] W. Wu, X. Xiao, and X. Huang, "The effect of battery design parameters on heat generation and utilization in a Li-ion cell," *Electrochimica Acta,* vol. 83, pp. 227-240, 2012.

[11] R. Srinivasan, A. C. Baisden, B. G. Carkhuff, and M. H. Butler, "The five modes of heat generation in a Li-ion cell under discharge," *Journal of Power Sources,* vol. 262, pp. 93-103, 2014.

[12] A. Eddahech, O. Briat, and J.-M. Vinassa, "Lithium-ion battery heat generation investigation based on calorimetric entropy measurements," in *2013 IEEE International Symposium on Industrial Electronics*, 2013: IEEE, pp. 1-5.

[13] X.-F. Zhang *et al.*, "Potentiometric measurement of entropy change for lithium batteries," *Physical Chemistry Chemical Physics,* vol. 19, no. 15, pp. 9833-9842, 2017.

[14] W. Shi, J. Zheng, J. Xiao, X. Chen, B. J. Polzin, and J.-G. Zhang, "The effect of entropy and enthalpy changes on the thermal behavior of Li-Mn-rich layered composite cathode materials," *Journal of The Electrochemical Society,* vol. 163, no. 3, p. A571, 2016.

[15] R. Srinivasan and B. G. Carkhuff, "Empirical analysis of contributing factors to heating in lithium-ion cells: Anode entropy versus internal resistance," *Journal of power sources,* vol. 241, pp. 560-566, 2013.

[16] K. Smith and C.-Y. Wang, "Power and thermal characterization of a lithium-ion battery pack for hybrid-electric vehicles," *Journal of power sources,* vol. 160, no. 1, pp. 662-673, 2006.
[17] G. Nagasubramanian, "Electrical characteristics of 18650 Li-ion cells at low temperatures," *Journal of applied electrochemistry,* vol. 31, pp. 99-104, 2001.
[18] S. Zhang, K. Xu, and T. Jow, "The low temperature performance of Li-ion batteries," *Journal of Power Sources,* vol. 115, no. 1, pp. 137-140, 2003.
[19] W. Wu, W. Wu, X. Qiu, and S. Wang, "Low-temperature reversible capacity loss and aging mechanism in lithium-ion batteries for different discharge profiles," *International journal of energy research,* vol. 43, no. 1, pp. 243-253, 2019.
[20] H.-P. Lin *et al.*, "Low-temperature behavior of Li-ion cells," *Electrochemical and Solid-State Letters,* vol. 4, no. 6, p. A71, 2001.
[21] K. Uddin, S. Perera, W. D. Widanage, and J. Marco, "Characterising Li-ion battery degradation through the identification of perturbations in electrochemical battery models," *World Electric Vehicle Journal,* vol. 7, no. 1, pp. 76-84, 2015.
[22] S. Herreyre, O. Huchet, S. Barusseau, F. Perton, J. Bodet, and P. Biensan, "New Li-ion electrolytes for low temperature applications," *Journal of power sources,* vol. 97, pp. 576-580, 2001.
[23] M. Smart, B. Ratnakumar, L. Whitcanack, K. Chin, M. Rodriguez, and S. Surampudi, "Performance characteristics of lithium ion cells at low temperatures," *IEEE aerospace and electronic systems magazine,* vol. 17, no. 12, pp. 16-20, 2002.
[24] J. Li, C. F. Yuan, Z. H. Guo, Z. A. Zhang, Y. Q. Lai, and J. Liu, "Limiting factors for low-temperature performance of electrolytes in LiFePO4/Li and graphite/Li half cells," *Electrochimica acta,* vol. 59, pp. 69-74, 2012.
[25] L. Liao *et al.*, "Effects of temperature on charge/discharge behaviors of LiFePO4 cathode for Li-ion batteries," *Electrochimica Acta,* vol. 60, pp. 269-273, 2012.
[26] S. Zhang, K. Xu, and T. Jow, "Electrochemical impedance study on the low temperature of Li-ion batteries," *Electrochimica acta,* vol. 49, no. 7, pp. 1057-1061, 2004.
[27] A. Vlahinos and A. A. Pesaran, "Energy efficient battery heating in cold climates," *SAE Transactions,* pp. 826-833, 2002.
[28] C.-Y. Wang *et al.*, "Lithium-ion battery structure that self-heats at low temperatures," *Nature,* vol. 529, no. 7587, pp. 515-518, 2016.
[29] T. Stuart and A. Hande, "HEV battery heating using AC currents," *Journal of Power Sources,* vol. 129, no. 2, pp. 368-378, 2004.
[30] L. Zhang, W. Fan, Z. Wang, W. Li, and D. U. Sauer, "Battery heating for lithium-ion batteries based on multi-stage alternative currents," *J Energy Storage,* vol. 32, p. 101885, 2020.
[31] J. Zhang, H. Ge, Z. Li, and Z. Ding, "Internal heating of lithium-ion batteries using alternating current based on the heat generation model in frequency domain," *Journal of Power Sources,* vol. 273, pp. 1030-1037, 2015.
[32] T. Özdemir, "Thermal Behavior of Lithium-ion Batteries Under Normal and Abuse Operating Conditions," PhD., Graduate School of Science and Engineering, Hacettepe University, 2022.

[33] M. Doyle, T. F. Fuller, and J. Newman, "Modeling of galvanostatic charge and discharge of the lithium/polymer/insertion cell," *Journal of the Electrochemical society,* vol. 140, no. 6, p. 1526, 1993.
[34] J. Newman and W. Tiedemann, "Porous-electrode theory with battery applications," *AIChE Journal,* vol. 21, no. 1, pp. 25-41, 1975.
[35] S. Tippmann, D. Walper, L. Balboa, B. Spier, and W. G. Bessler, "Low-temperature charging of lithium-ion cells part I: Electrochemical modeling and experimental investigation of degradation behavior," *Journal of Power Sources,* vol. 252, pp. 305-316, 2014.
[36] H. Ge *et al.*, "Investigating lithium plating in lithium-ion batteries at low temperatures using electrochemical model with NMR assisted parameterization," *Journal of The Electrochemical Society,* vol. 164, no. 6, p. A1050, 2017.
[37] Y. Ye, Y. Shi, N. Cai, J. Lee, and X. He, "Electro-thermal modeling and experimental validation for lithium ion battery," *Journal of Power Sources,* vol. 199, pp. 227-238, 2012.
[38] W. Fang, O. J. Kwon, and C. Y. Wang, "Electrochemical–thermal modeling of automotive Li-ion batteries and experimental validation using a three-electrode cell," *International journal of energy research,* vol. 34, no. 2, pp. 107-115, 2010.
[39] T. Kulova, A. Skundin, E. Nizhnikovskii, and A. Fesenko, "Temperature effect on the lithium diffusion rate in graphite," *Russian Journal of Electrochemistry,* vol. 42, pp. 259-262, 2006.
[40] L. Saw, Y. Ye, and A. Tay, "Electrochemical–thermal analysis of 18650 Lithium Iron Phosphate cell," *Energy Conversion and Management,* vol. 75, pp. 162-174, 2013.
[41] G. Fan, K. Pan, M. Canova, J. Marcicki, and X. G. Yang, "Modeling of Li-Ion cells for fast simulation of high C-rate and low temperature operations," *Journal of The Electrochemical Society,* vol. 163, no. 5, p. A666, 2016.
[42] B. Suthar, P. W. Northrop, D. Rife, and V. R. Subramanian, "Effect of porosity, thickness and tortuosity on capacity fade of anode," *Journal of The Electrochemical Society,* vol. 162, no. 9, p. A1708, 2015.
[43] J. Li *et al.*, "An electrochemical–thermal model based on dynamic responses for lithium iron phosphate battery," *Journal of Power Sources,* vol. 255, pp. 130-143, 2014.
[44] K. G. Gallagher, D. W. Dees, A. N. Jansen, D. P. Abraham, and S.-H. Kang, "A volume averaged approach to the numerical modeling of phase-transition intercalation electrodes presented for LixC6," *Journal of The Electrochemical Society,* vol. 159, no. 12, p. A2029, 2012.
[45] J. Landesfeind and H. A. Gasteiger, "Temperature and concentration dependence of the ionic transport properties of lithium-ion battery electrolytes," *Journal of The Electrochemical Society,* vol. 166, no. 14, pp. A3079-A3097, 2019.
[46] T. G. Zavalis, M. Behm, and G. Lindbergh, "Investigation of Short-Circuit Scenarios in a Lithium-Ion Battery Cell," *Journal of The Electrochemical Society,* vol. 159, no. 6, p. A848, 2012/04/16 2012, doi: 10.1149/2.096206jes.

[47] L. O. Valøen and J. N. Reimers, "Transport properties of LiPF6-based Li-ion battery electrolytes," *Journal of The Electrochemical Society,* vol. 152, no. 5, p. A882, 2005.
[48] K. Kumaresan, G. Sikha, and R. E. White, "Thermal Model for a Li-Ion Cell," *Journal of The Electrochemical Society,* vol. 155, no. 2, A164, 2008, doi: 10.1149/1.2817888.
[49] G. Gwak and H. Ju, "Multi-scale and multi-dimensional thermal modeling of lithium-ion batteries," *Energies,* vol. 12, no. 3, p. 374, 2019.
[50] M. Rashid and A. Gupta, "Experimental assessment and model development of cycling behavior in Li-ion coin cells," *Electrochimica Acta,* vol. 231, pp. 171-184, 2017.
[51] S. Santhanagopalan, Q. Guo, P. Ramadass, and R. E. White, "Review of models for predicting the cycling performance of lithium ion batteries," *Journal of power sources,* vol. 156, no. 2, pp. 620-628, 2006.
[52] G. Richardson, I. Korotkin, R. Ranom, M. Castle, and J. Foster, "Generalised single particle models for high-rate operation of graded lithium-ion electrodes: systematic derivation and validation," *Electrochimica Acta,* vol. 339, p. 135862, 2020.
[53] P. Tagade *et al.*, "Bayesian calibration for electrochemical thermal model of lithium-ion cells," *Journal of Power Sources,* vol. 320, pp. 296-309, 2016.
[54] T. Hatchard, D. MacNeil, A. Basu, and J. Dahn, "Thermal model of cylindrical and prismatic lithium-ion cells," *Journal of The Electrochemical Society,* vol. 148, no. 7, p. A755, 2001.
[55] A. Fly, I. Kirkpatrick, and R. Chen, "Low temperature performance evaluation of electrochemical energy storage technologies," *Applied Thermal Engineering,* vol. 189, p. 116750, 2021.
[56] R. Benger, H. Wenzl, H.-P. Beck, M. Jiang, D. Ohms, and G. Schaedlich, "Electrochemical and thermal modeling of lithium-ion cells for use in HEV or EV application," *World Electric Vehicle Journal,* vol. 3, no. 2, pp. 342-351, 2009.
[57] Y. Shang, C. Zhu, G. Lu, Q. Zhang, N. Cui, and C. Zhang, "Modeling and analysis of high-frequency alternating-current heating for lithium-ion batteries under low-temperature operations," *Journal of Power Sources,* vol. 450, p. 227435, 2020.
[58] S. Drake, D. Wetz, J. Ostanek, S. Miller, J. Heinzel, and A. Jain, "Measurement of anisotropic thermophysical properties of cylindrical Li-ion cells," *Journal of Power Sources,* vol. 252, pp. 298-304, 2014.
[59] T. R. Ashwin, A. McGordon, and P. A. Jennings, "Electrochemical modelling of Li-ion battery pack with constant voltage cycling," *Journal of Power Sources,* vol. 341, pp. 327-339, 2017/02/15/ 2017, doi: https://doi.org/10.1016/j.jpowsour.2016.11.092.
[60] C. W. Lee, Y. Hong, M. Hayrapetyan, X. G. Yang, and Z. Xi, "Derivation and tuning of a solvable and compact differential–algebraic equations model for LiFePO4–graphite Li–ion batteries," *Journal of Applied Electrochemistry,* vol. 48, no. 3, pp. 365-377, 2018/03/01 2018, doi: 10.1007/s10800-018-1164-8.
[61] G. Ning and B. N. Popov, "Cycle Life Modeling of Lithium-Ion Batteries," *Journal of The Electrochemical Society,* vol. 151, no. 10, p. A1584, 2004/09/21 2004, doi: 10.1149/1.1787631.

[62] J. Remmlinger, M. Buchholz, T. Soczka-Guth, and K. Dietmayer, "On-board state-of-health monitoring of lithium-ion batteries using linear parameter-varying models," *Journal of Power Sources,* vol. 239, pp. 689-695, 2013.
[63] H. You, H. Dai, L. Li, X. Wei, and G. Han, "Charging Strategy Optimization at Low Temperatures for Li-Ion Batteries Based on Multi-Factor Coupling Aging Model," *IEEE Transactions on Vehicular Technology,* vol. 70, no. 11, pp. 11433-11445, 2021.
[64] "Panasonic NCR19650B Lithium-ion Battery Datasheet." https://pdf1.alldatasheet.com/datasheet-pdf/view/597043/PANASONICBATTERY/NCR18650B.html (accessed 01.01.2023, 2023).
[65] Y. Ji, Y. Zhang, and C.-Y. Wang, "Li-ion cell operation at low temperatures," *Journal of The Electrochemical Society,* vol. 160, no. 4, p. A636, 2013.
[66] D. Chalise, K. Shah, T. Halama, L. Komsiyska, and A. Jain, "An experimentally validated method for temperature prediction during cyclic operation of a Li-ion cell," *International Journal of Heat and Mass Transfer,* vol. 112, pp. 89-96, 2017.
[67] S. Zhang, K. Xu, and T. Jow, "Low temperature performance of graphite electrode in Li-ion cells," *Electrochimica acta,* vol. 48, no. 3, pp. 241-246, 2002.
[68] H. Lundgren, M. Behm, and G. Lindbergh, "Electrochemical characterization and temperature dependency of mass-transport properties of LiPF6 in EC: DEC," *Journal of The Electrochemical Society,* vol. 162, no. 3, p. A413, 2014.
[69] K. A. Murashko, J. Pyrhönen, and J. Jokiniemi, "Determination of the through-plane thermal conductivity and specific heat capacity of a Li-ion cylindrical cell," *International Journal of Heat and Mass Transfer,* vol. 162, p. 120330, 2020.
[70] T. Özdemir, A. Amini, Ö. Ekici, and M. Köksal, "Experimental assessment of the lumped lithium ion battery model at different operating conditions," *Heat Transfer Engineering,* vol. 43, no. 3-5, pp. 314-325, 2021.
[71] D. Wang, H. Huang, Z. Tang, Q. Zhang, B. Yang, and B. Zhang, "A lithium-ion battery electrochemical–thermal model for a wide temperature range applications," *Electrochimica Acta,* vol. 362, p. 137118, 2020.

APPENDICES

Appendix 1: Combined Parameters Study

In previous chapters, results of changing a single parameter are investigated. Some of the parameters were thought to be best left unchanged because the corresponding base model values are in agreement with the literature. However, the effects of the multiple parameters varied simultaneously were still investigated. Table A.1. summarizes the ratios of combined parameters in this part of the study. It should be noted that, in this part of the study, parameters were changed without considering their realistic behavior at the low temperature operations. Fig. A.1. and Fig. A.2. show the combined parameters results.

Table A.1. Ratios of Combined Parameter Study

Changed Parameter	**Ratio**
Electrolyte Diffusion Coefficient,	110%
Electrolyte Ionic Conduction Coefficient	90%
Electrolyte Transport Number	90%
Electrolyte Activity Dependence	90%
Cathode Bruggeman Coefficient	110%
Anode Bruggeman Coefficient	80%
Separator Bruggeman Coefficient	110%
SEI Film Resistance	280%

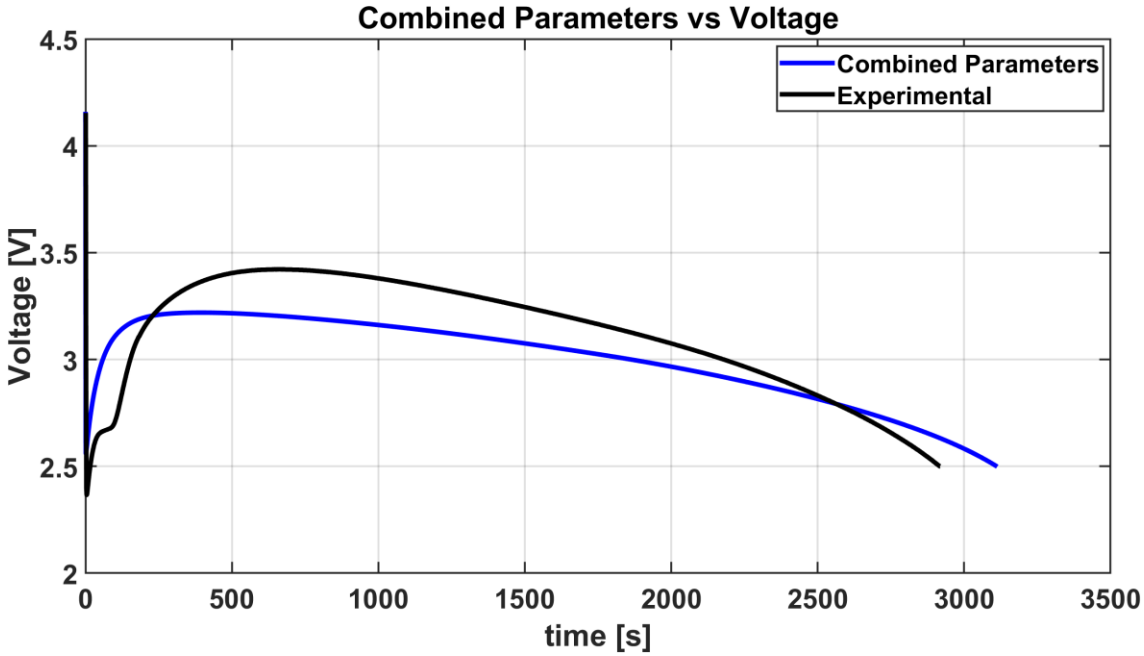

Figure A.1. Combined Parameters vs Voltage

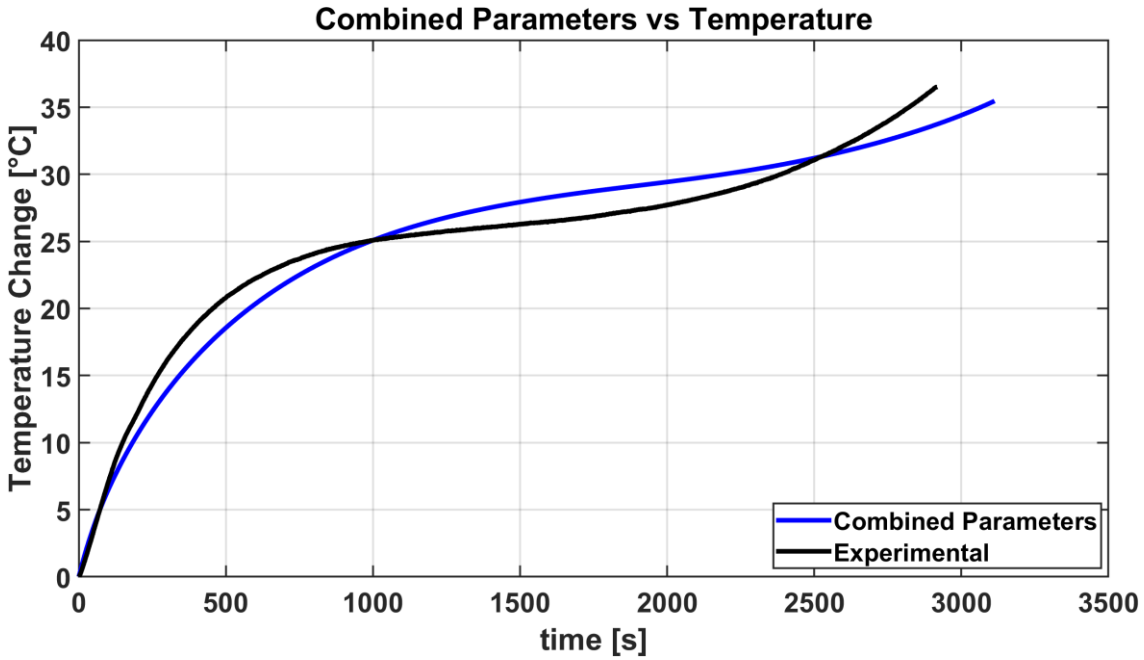

Figure A.2. Combined Parameters vs Temperature

In the liquid phase, electrolyte diffusion coefficient of 110% of the base model value, electrolyte ionic conduction coefficient of 90% of the base model value, electrolyte transport number of 90% of the base model value, activity dependence of 110% of the base model value were used. For correcting porous media

behaviors, Bruggeman coefficients of 110% of the base model value for the positive electrode, 80% for the negative electrode and 110% for the separator were used. SEI film resistance of 280% of the Eqn. (35) was deployed. In the solid phase, diffusion coefficients and reaction rate constants were left unchanged. Because their effect on the battery performance were minimal in comparison to the other parameters.

Simulation of combined parameters showed better accuracy than any of the parameter individually changed. Unlike the individual analysis, SEI film resistance was increased as much as 280% of the initial value. It was chosen to be 280% entirely as a solution to the quick drop of the voltage at the very start. The other parameters were chosen to be inside of the range of the sensitivity analysis performed earlier. Combined parameters analysis performs somewhat linearly after the voltage rebound, compared to the experimental results. It could be due to lack of temperature dependence in the characterization of the parameters. In the model, varied transport number and activity dependence and other unchanged parameters such as solid phase diffusion of positive electrode, and reaction rate constants were only concentration dependent. Thermal parameters such as specific heat capacities, and thermal conductivities of all battery components, including battery casing and current collectors, were assumed to be constant. Since the concentration was changing linearly throughout the discharge, it can be argued that this is reason that the model was unable to predict battery performance at -20°C during 1C discharge.

In light of the results, it is crucial to recognize that temperature dependence of the lithium-ion battery properties has significant effect on the numerical modeling. Mostly, some of the utilized model parameters in the literature are considered as only lithium concentration dependent since the studies were generally conducted at a single temperature condition and the limited effects of those concentration dependent parameters could get satisfactory results. However, operations at low temperatures and high C-rates get the lithium-ion batteries to heat up exceptionally which makes the temperature dependent modeling essential.